Semiconductor Optoelectronics
ISSN: 1001-5868

INFLUENCE OF CADMIUM ON STRUCTURAL, MORPHOLOGICAL AND MAGNETIC PROPERTIES OF COBALT NICKEL FERRITE

A V Bagde
Department of physics, Dhote Bandhu Science College, Gondia, Maharashtra, India
Email-akashbagde24@rediffmail.com

D S Choudhary
Department of Physics, Dhote Bandhu Science College, Gondia, India
Email- dschoudhary@dbscience.org

A M Shahare
Department of Physics, Dhote Bandhu Science College, Gondia, India
Email- amshahare@gmail.com

Y S Bopche
Department of Physics, Dhote Bandhu Science College, Gondia, India
Email- ysbopche@dbscience.org

ABSTRACT:

In the present study, we have explored the influence of substit0ution of Cadmium (Cd^{2+}) ions on structural, morphological, and magnetic properties of Cobalt-Nickel (Co-Ni) spinel ferrites synthesized by the Sol-Gel Combustion method. The lattice constants exhibited an increasing trend with respect to Cadmium contents. XRD study found hindered Crystallite size with increasing Cd concentration. Field Emission Scanning Electron Microscopy (FE-SEM) and HR-TEM was used to observe the surface morphology. The average grain size estimated from the FE-SEM microstructures was found to be in the range 148 – 46 nm for the studied samples. HR-TEM predicts the grain size in the range of 112-44 nm. Fourier transform infrared (FT-IR) spectra identified two prominent absorption bands from 597.53–574.82 cm^{-1} and 417.18–420.27 cm^{-1} corresponding to the tetrahedral and octahedral voids, respectively. X-ray density, Bulk density, hopping length show increasing trend, while porosity is decreasing with Cadmium content. The saturation magnetization (M_s), Remanent magnetization (M_r) observed to be increasing upto $x = 0.2$ concentration of Cd and decreasing thereafter due to spin canting effect. The maximum saturation magnetization (Ms) was found to be 78 emu/gm for the sample with x = 0.2. Total magnetic moment (n_B) follow the similar trend as M_s. Coercivity is reducing linearly with increasing Cd doping.

1. Introduction:

In his popular lecture “There is plenty of room at the bottom” in 1959 at the annual

American Physical Society meeting at Caltech, Richard Feynman conceptualized the direct manipulation of individual atoms as a more robust form of synthetic chemistry. With its golden period in 1980's, Nanotechnology has revolutionized our industries and our lives since then. Spinel ferrite nanocrystals demonstrate magnetic properties due to the presence of magnetic ions on its tetrahedral (A) and octahedral (B) sites and that also depends on the relative strength of their inter sub lattice (J_{AB}) and inter sub lattice (J_{BB}, J_{AA}) interactions [1]. Any changes in the numbers of the magnetic ions in both the sites, certainly affect the magnetic properties. Literature review revealed that spinel ferrite properties are greatly influenced by the method of synthesis, so the different methods of nanoferrites like sol–gel method, co-precipitation method, ball milling, microemulsion processing, etc. received special attention [2] [3] [4] [5]. Among other Spinel ferrites, Co-Ni ferrite nanostructures exhibit remarkable electromagnetic properties allowed them to be striking applicants for high-frequency electronic devices in telecommunication applications [6].

Nickel ferrite is a well-known soft magnetic material with inverse spinel structure, where A site contains Fe^{3+} ions only but B sites contains both Ni^{2+} and Fe^{3+} ions [7], which have a low value of coercivity and saturation magnetisation [8-9]. Cobalt belongs to a hard magnetic material category, so its substitution on nickel ferrite, exhibits large magneto-crystalline anisotropy constant and high intrinsic coercivity [10-11]. Due to combined hard and soft nature of the ferrites due to Nickel and cobalt respectively, the modified magnetic properties make Cobalt Nickel ferrite nanocrystals advantageous for application in biomedical, data storage, information delivery devices, magnetoelectric materials and as microwave absorption material [12-14]. Hosseini et al. [15] studied the catalytic activity of Ni–Co ferrite on the growth of carbon nanotube and indicated an inverse spinel structure for Ni–Co ferrite. This suggests that Ni^{2+} and Co^{2+} cations resides the octahedral sites while Fe^{3+} cations occupy both octahedral and tetrahedral sites likewise.

The Cadmium ion substitution fascinatingly alters and enhances ferrite's structural, electrical and magnetic properties. Bhukal et. al. [16] investigated Cd^{2+} ion substituted nano-crystalline cobalt–zinc ferrites and results revealed that the saturation magnetization, coercivity and anisotropy constant decrease with increase in the cadmium concentration due to redistribution of ions on tetrahedral (A) and octahedral (B) sites . Singhal et. al. [17] found increased saturation magnetization up to x = 0·4 and decreases when the value of x is > 0·4 due to spin canting and existence of Yafet–Kittel (Y–K) angle. Present work aims to study the impact of Cadmium doping on cobalt-nickel ferrite's structural, morphological and magnetic properties.

2. Experimental

Mixed Cadmium doped Co-Ni ferrites having chemical formula $Co_{0.6-x}\ Ni_{0.4}\ Cd_x\ Fe_2\ O_4$ with x=0.00 to 0.5 with stepping of 0.1 are synthesized by sol-gel auto combustion technique. All chemicals used are of analytical grade. Copper nitrate [$Cu(NO_3)_2 \cdot 3H_2O$], nickel nitrate [$Ni(NO_3)_2 \cdot 6H_2O$], cadmium nitrate [$Cd(NO_3)_2 \cdot 4H_2O$], iron nitrate [$Fe(NO_3)_3 \cdot 9H_2O$] are taken in stoichiometric ratios and citric acid [$C_6H_8O_7 \cdot H_2O$] is used a chelating agent. Mixed solutions of Metal nitrates and citric acid are evanesced in deionized water which concedes aqueous solution. It is mixed with 1:1 M ratio of nitrate to citric acid. The pH of mixed solution gets attuned to 7 using AR grade ammonia solution. The mixture is then neutralized with aqueous ammonia and heated upto 80°C under constant stirring to transform into to gel form. When

burst into flames at any point of the gel, the dried gel is burnt in a self-propagating combustion manner till all gel are wholly burnt out to form a fluffy loose ash auxiliary, it is further proceed in borosil glass beaker upon a hot plate for supplementary dry process. The ash is lightly ground and is calcined at 800°C for 8 h so that the some impurity will evolve. Using X-ray diffraction (XRD), phase identification, crystalline size and lattice parameter have been characterized with Cu-Kα radiation. The crystalline size is calculated from peak broadening using Scherrer formula. Microstructure of the sintered specimens has been analyzed by scanning electron microscopy (SEM). Static magnetic properties like Saturation magnetization (Ms), remanent magnetization (Mr), coercivity (Hc), remanent ratio (Mr/Ms), etc, of the samples are measured at room temperature using vibration sample magnetometer (VSM), operating with magnetic field of 20 kOe.

3. Result and Discussion

3.1 X-ray Diffraction

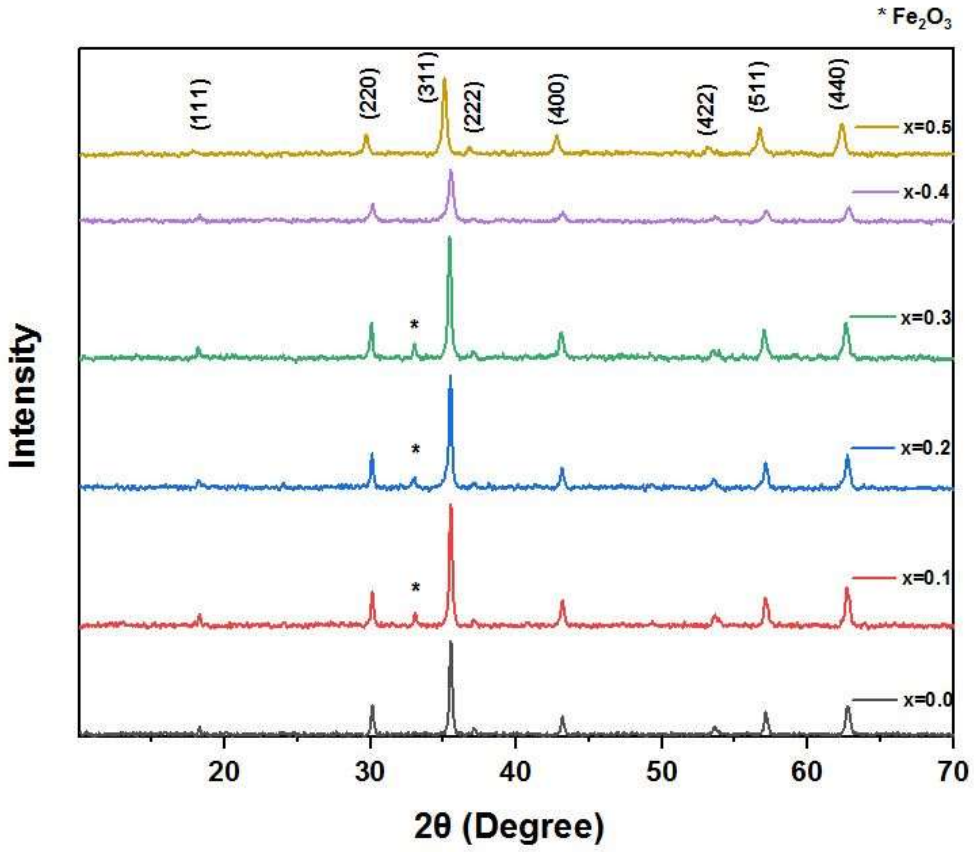

Fig. 1(a): Diffraction Pattern of Cd substituted Co-Ni Ferrite

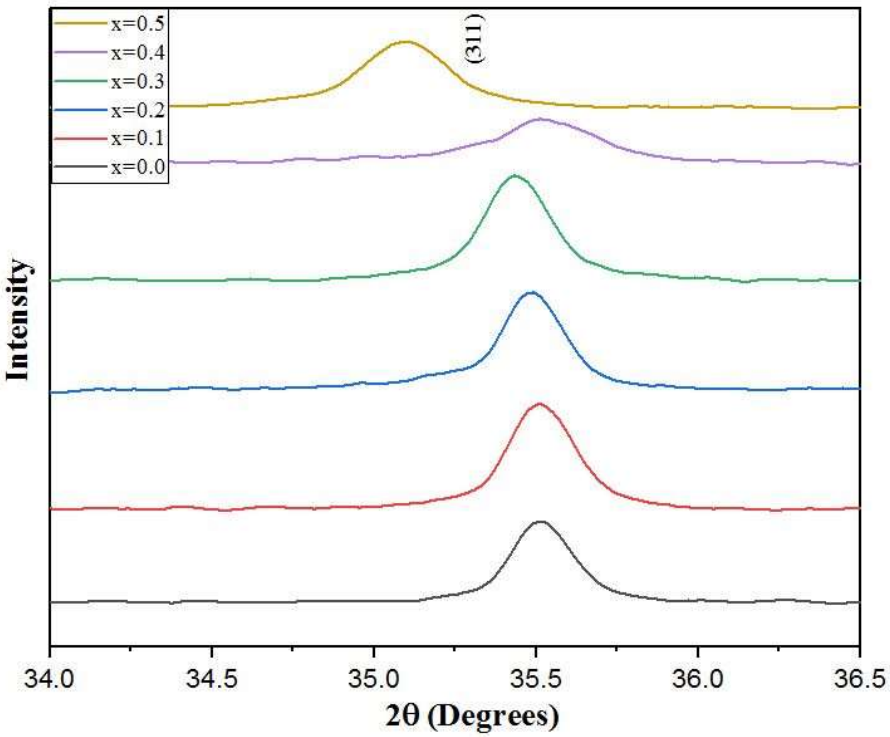

Fig. 1(b): Shifting of (311) peak to lower 2θ values with Cd concentration

The X-ray diffraction patterns of $Co_{0.6-x}$ $Ni_{0.4}$ Cd_x Fe_2 O_4 ($x = 0.0, 0.1, 0.2, 0.3, 0.4$ and 0.5) are illustrated in **Fig. 1(a)**. The observed XRD patterns were matched and indexed with the help of PDF no. (44-1485) and (22-1086) for Ni and Co ferrites The formation of the cubic structure of spinel ferrites have been established by the presence of peaks in XRD structure conforming to miller indices (111), (220), (311), (222), (422), (511), (440), (620). The inter planner distance d for the highest intensity peak has been calculated using Bragg's law [18]. The most dominant peak (311), at around 35°, confirms the formation of cubic spinel structure with a space group of *Fd-3m*. The peaks are well resolved and clearly indicate the polycrystalline nature of the ferrite. A prominent feature in these patterns is that the broadening of the peaks increases continuously with increasing cadmium substitution in relation to the ferrite without cadmium, indicating that the cadmium addition reduces the crystallite size of the Co–Ni ferrite. It can be seen from **Fig. 1(b)** that Cd doping caused a shift of XRD patterns to lower diffraction (2θ) angles. However, there are two additional humps in the XRD patterns of the x=0.1, 0.2, and 0.3 samples which can be associated with impurity phase Fe_2O_3 as indicated in Fig. 1(a) [19]. The slight change in the position of XRD peaks with varying dopant concentration is caused by the nature of the metal cations, their ionic radius, band energy and their favorable sites [20]. The observed and calculated values of interplanar distance d are in good agreement with each other. The lattice constant $'a'$ (Å) for all the samples was calculated using the prominent (311) peak using the equation,

$$a = d_{hkl}\sqrt{h^2 + k^2 + l^2}$$

XRD pattern of the samples reveals the shifting of the peak positions toward lower angle side with respect to increase in Cd content which is indicative of the fact that the lattice parameter increased with Cd doping. The lattice constants of all the samples observed are listed

in **Table 1**. Lattice constant values are found to be in the range 8.3719 Å to 8.4742 Å. From this table it is observed that the lattice constant of $Co_{0.6-x}$ $Ni_{0.4}$ Cd_x Fe_2 O_4 prepared by autocombustion method is increasing with respect to Cd content. The variation of lattice constants of Co-Ni ferrites as a function of Cd^{2+} content is presented in **Fig. 2**. From this figure, it is observed that the lattice constant increases with increase in Cd^{2+} content. The increase in lattice constant with Cd^{2+} content can be attributed to larger ionic radii of Cd^{2+} (1.03 Å) ion which is replacing the smaller ionic radii of Co^{2+} (0.84 Å) and Fe^{3+} (0.67 Å) ion in the spinel lattice from tetrahedral (A) site to octahedral (B) site in Co–Ni ferrite [21]. The variation in the lattice parameter indicates that the system under study conform the Vegard's law. According to which, the deviations in the values of lattice parameters are due to larger ionic radii of doped Cd^{2+} (1.03 Å) ion compared to constituent Co^{2+} (0.84 Å) and Fe^{3+} (0.67 Å) ions. Similar behavior is also reported by other researchers also [22-27].

Table 1: Structural Parameters of Cd substituted Co-Ni Ferrite

Concentration (x)	Crystallite Size (D) (nm)	Lattice Constant (a) (Å)	X-Ray Density (D_x) (g/cm3)	Bulk Density(D_b) (g/cm3)	Porosity (P) (%)	Hopping Length	
						L_A (Å)	L_B (Å)
0	31.38	8.37531	5.1197	2.2	57.03	3.6266	2.9612
0.1	25.40	8.37532	5.4242	2.31	57.41	3.6266	2.9612
0.2	24.77	8.38468	5.5451	2.54	54.19	3.6307	2.9644
0.3	24.68	8.39248	5.6314	2.98	47.08	3.6340	2.9672
0.4	20.70	8.37191	5.7676	3.2	44.52	3.6251	2.9599
0.5	20.33	8.47418	5.9151	3.28	44.55	3.6694	2.9961

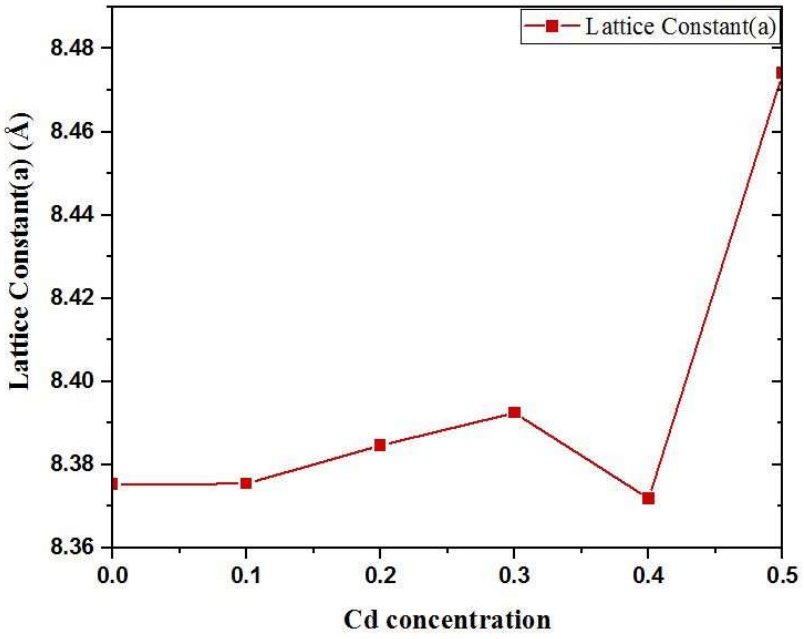

Fig. 2: Variation of Lattice constant with respect to Cd concentration

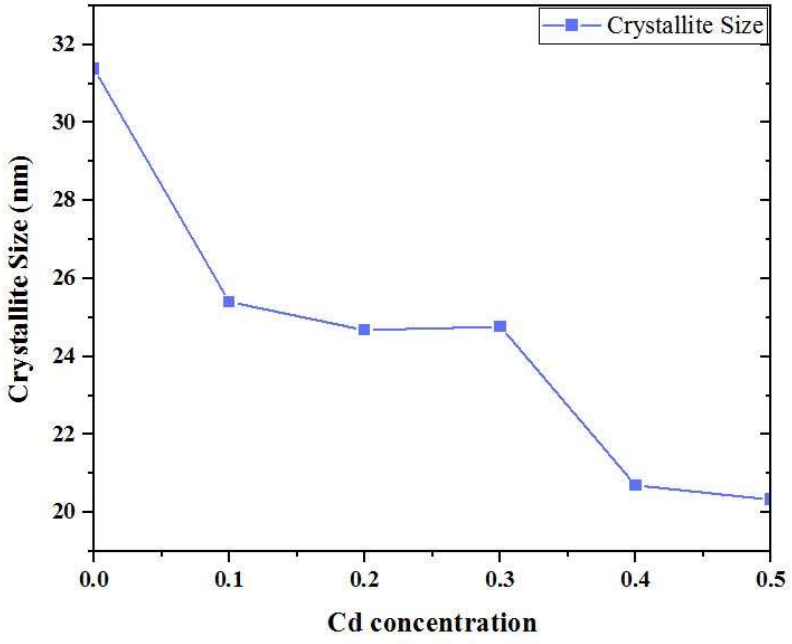

Fig. 3: Variation of Crystallite Size with respect to Cd concentration

A clear variation is observed in FWHM of XRD diffractogram, which is reflected in the calculations of the crystallite sizes. **Table 1**, shows the variation of the average crystalline sizes for the cubic spinel phase. The average crystallite size for all samples of $Ni_{0.4}Co_{0.5-x}Cd_xFe_2O_4$ using (311) plane was determined by Debye Scherrer formula [28],

$$D = \frac{0.94\lambda}{\beta cos\theta}$$

where λ is the wavelength of X-ray, β is the full width at half maxima, and θ is the Bragg's diffraction angle. The average crystallite size 'D' is presented in the **Table 1**. From this table it is observed that, the crystallite size of the sample lies in the nano particle regime with the range 20.33 to 31.38 nm. It is observed that there is a homogeneous decrease in the crystallite size as the Cd $^{2+}$ ion concentration surges [29]. The average particle size of $Co_{0.6}\,Ni_{0.4}\,Fe_2\,O_4$ is 31.38 nm, which decreases with increasing Cd $^{2+}$ ion concentration and becomes 20.33 nm in the case of $Co_{0.1}\,Ni_{0.4}\,Cd_{0.5}\,Fe_2\,O_4$. It is understood from the above observation that the crystal growth is hindered due to the presence of Cd $^{2+}$ ions in the spinel ferrite [30-32].

The hopping length L_A and L_B, which are respectively defined as the gap between the magnetic ions in A-sites and in B- sites, can also be evaluated by considering the experimental value of lattice constant, using the following equations, as given in Table [1]

$$L_A = \left(\frac{\sqrt{3}}{4}\right)a$$

$$L_B = \left(\frac{\sqrt{2}}{4}\right)a$$

It has been found that both L_A and L_B increases with doping of cadmium on Co-Ni Ferrite, as there is an increase of lattice constant value for Co-Ni Ferrite nanocrystals, which is attributed to the difference in the ionic radii of constituent ions [20] [33].

Role of density in ferrites is very influential in determining its magnetic and electrical properties. It is well-known that high permeability can be achieved through enhanced density of the ferrites. In the present work, X-ray density (D_x) for each sample is calculated using the relation,

$$D_x = \frac{8M}{Na^3}$$

where M is the molecular weight of the sample, N is the Avogadro's number and a is the lattice constant. Also, the bulk density (D_B), of the samples was measured using the relation,

$$D_B = \frac{m}{V}$$

where m is the mass of the bulk sample in grams, and V is its volume in cubic centimeters. The variation of X-ray density (D_x) and bulk density (D_B) with respect to Cd $^{2+}$ concentration (x) is presented in Table [1]. The bulk and X-ray densities as a function of Cd content are shown in Fig. 4. It is observed that the X-ray density increases almost linearly with increasing Cd concentration [34]. The bulk density imitates almost the similar general behavior as of X-ray density. The results reveal that substitution of Cd has a pronounced effect on the densification of the $CoNiFe_2O_4$ [35, 25]. The Bulk densities (D_B) are lower than X-ray densities D_X, which is expected due to existence of cracks and pores in a sintered specimen during sintering process on the macroscopic scale and vacancies in the lattice on the atomic scale [36-37]. The enhancement in x-ray density is attributed to the higher atomic weight of cadmium (112.4 a.m.u) than cobalt (58.93 a.m.u). Increase in lattice parameter and enhanced cell volume may also made contribution to the improved X-ray density [38-39].

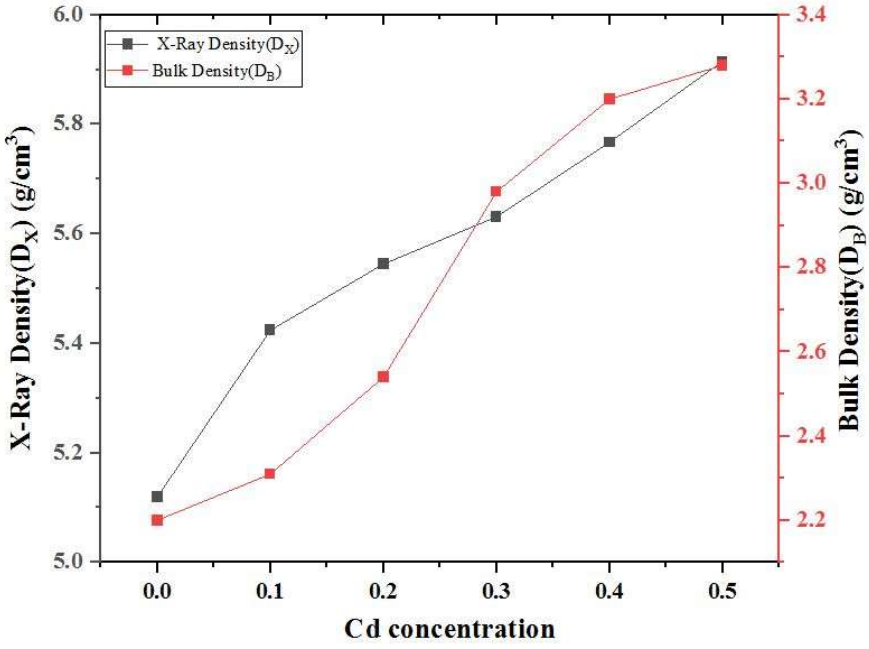

Fig 4. Variation of X-ray density and bulk density with respect to Cd content

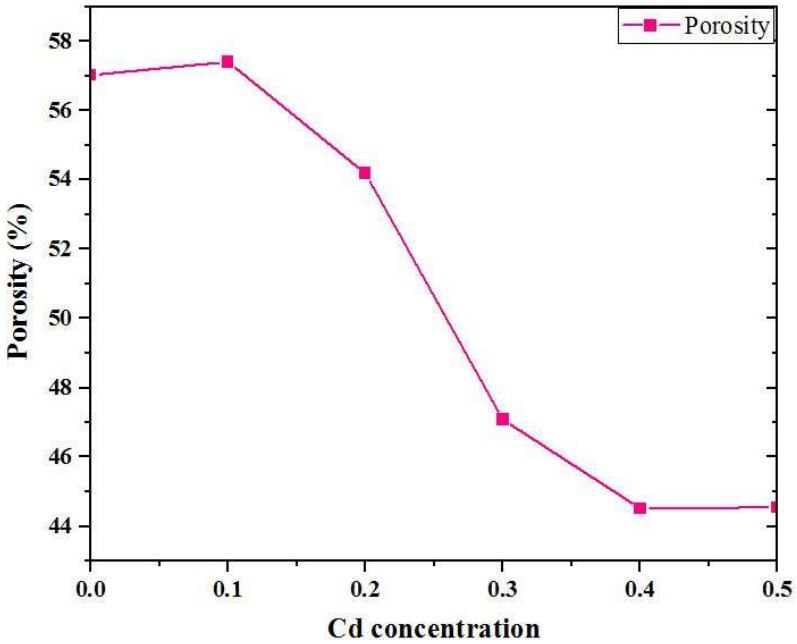

Fig. 5. Variation of Porosity with respect to Cd content

The porosity (P) of the samples is calculated by using the relation [40],

$$P = 1 - \frac{D_B}{D_x}$$

where D_B is the bulk density and D_x is the X–ray density. The porosity of $Ni_{0.4}Co_{0.5-x}Cd_xFe_2O_4$ nanoferrites are presented in Table 1. It is displayed in Table 1 that the porosity of samples is inversely proportional to measured density of samples. The data reveals the reduced porosity

with increase in Cd $^{2+}$ content. The decrease in porosity may be due to the formation of more oxygen vacancies with the substitution of Cd ions in the samples and virtually less cation are formed. [41-43].

3.2 FTIR spectroscopy

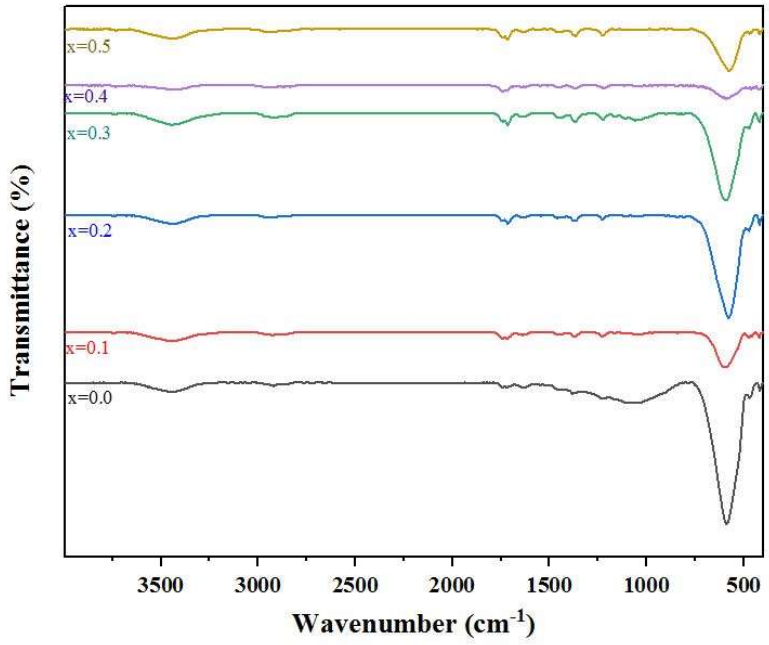

(a)

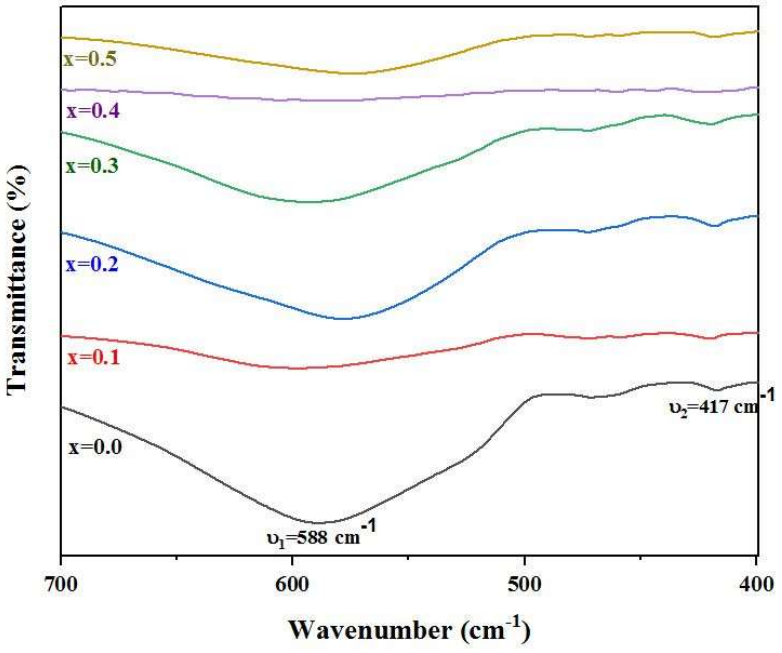

(b)

Fig. [6]: FTIR spectrogram of $Co_{0.6-x}$ $Ni_{0.4}$ Cd_x Fe_2 O_4 (with x=0.0, 0.1, 0.2, 0.3, 0.4 and 0.5) ferrites. (a) For 400 - 4000 cm^{-1} and (b) 400 - 700 cm^{-1} wavenumber range.

FTIR analysis has been used to study the occurrence of various absorption bands in the spectra and analyzed on the basis of different cations present on tetrahedral (A-) and octahedral (B-) sites of spinel lattice [44]. It is also useful in determining the local symmetry in crystalline solids, non-crystalline solids, ordering phenomenon in spinels, presence/absence of Fe^{2+} ions and also to determine force constants and elastic moduli of ferrite systems [45-47].

According to Waldron's group theoretical considerations [45], the unit cell of cubic spinel can be formed by tetrahedral (A) and octahedral (B) sites and there exist two fundamental I.R. active vibrational modes in the spinal structure. Accordingly, band ν_1 can be assigned to stretching vibrations of the tetrahedral metal–oxygen (Me–O) bond while band ν_2 is associated with the metal–oxygen vibrations in octahedral sites. The spectral difference is caused by the variation in band lengths in the octahedral and tetrahedral sites. Higher value of band ν_1, than that of ν_2 reveals that the normal vibration mode of the tetrahedral complexes is more than that of the corresponding octahedral sites. This may be the consequence of a shorter bond length in the tetrahedral site in comparison to that in the octahedral one.

Fig. [6] shows the FTIR absorption bands of $Co_{0.6-x}\ Ni_{0.4}\ Cd_x\ Fe_2\ O_4$ (with x=0.0, 0.1, 0.2, 0.3, 0.4 and 0.5) ferrite systems, which were recorded at room temperature in the wavenumber range of 400 - 4000 cm^{-1}. It is a well-known that normal and inverse cubic spinels have four fundamental IR bands. Two of them, around 600 and 400 cm^{-1}, are common for almost all spinel-type ferrites. The values of absorption frequencies of all samples are given in Table [2]. The difference in the band's position is due to the change in the bond length of Fe^{3+}–O_2 in the A- and B-sites. The appearance of these two absorption frequencies in the samples also confirms the formation of the spinel structure. However, the band's position is influenced by factors for instance preparation method, grain size, and annealing conditions [48]. In the present investigation, the characteristic bands ν_1 and ν_2 were found to be located within the ranges 574–597 and 417–420 cm^{-1}, owing to the fundamental vibrational mode of tetrahedral (A) and octahedral (B) position of ferrites [49-51]. Depending on the mass of the metal cations and strength of the bond between metal cation and oxygen, absorption occurred at different frequencies. In all spinel ferrites, two main broad metal oxygen bands are seen in the FTIR spectra [45, 52-54]. The first and strongest absorption band (ν_1), observed in the range $574-597\ cm^{-1}$, corresponds to intrinsic stretching vibrations of the metal ion at the tetrahedral site, (M_{tetra} - O; $Cd^{2+}\leftrightarrow$ O) [34], whereas the lowest band (ν_2), that observed in the range $417-420\ cm^{-1}$ is assigned to octahedral metal stretching vibration (M_{octa} - O; $Fe^{3+}\leftrightarrow$ O and $Co^{2+}\leftrightarrow$ O, $Ni^{2+}\leftrightarrow$ O) [45]. The band appearing at 3438 cm^{-1} Corresponds to O-H stretching vibration of H_2O; the special absorption peak at 2922 cm^{-1} corresponds to O-H group of citric acid; the band at 1377 cm^{-1} corresponds to antisymmetric NO_3 stretching vibrations and the band at 1639 cm^{-1} corresponds to carbo-oxalate anions [53-54].

It is known that an increase in site radius decreases the fundamental frequency and consequently the center frequency shift toward lower values. Co^{2+} ions occupied octahedral B sites in Cobalt-nickel ferrites; the substitution with Cd^{2+} ions decline the amount of Co^{2+} ions and redistributes Fe^{3+} ions from B site to A site [55]. In the present case, increase in site radius is expected due to replacement of smaller Co^{2+} ions (0.072 nm) by larger Cd^{2+} (0.097 nm)

ions. This is due to the fact that substituted Cd^{2+} ions preferentially occupy the A site only and the difference between the ionic radii of A-site Fe^{3+} (0.064 nm) and Cd^{2+} (0.097 nm) cations is much larger as compared to those of B-site Fe^{3+} (0.064 nm) and Co^{2+} (0.072 nm) cations [33].

3.3 Scanning electron microscopy

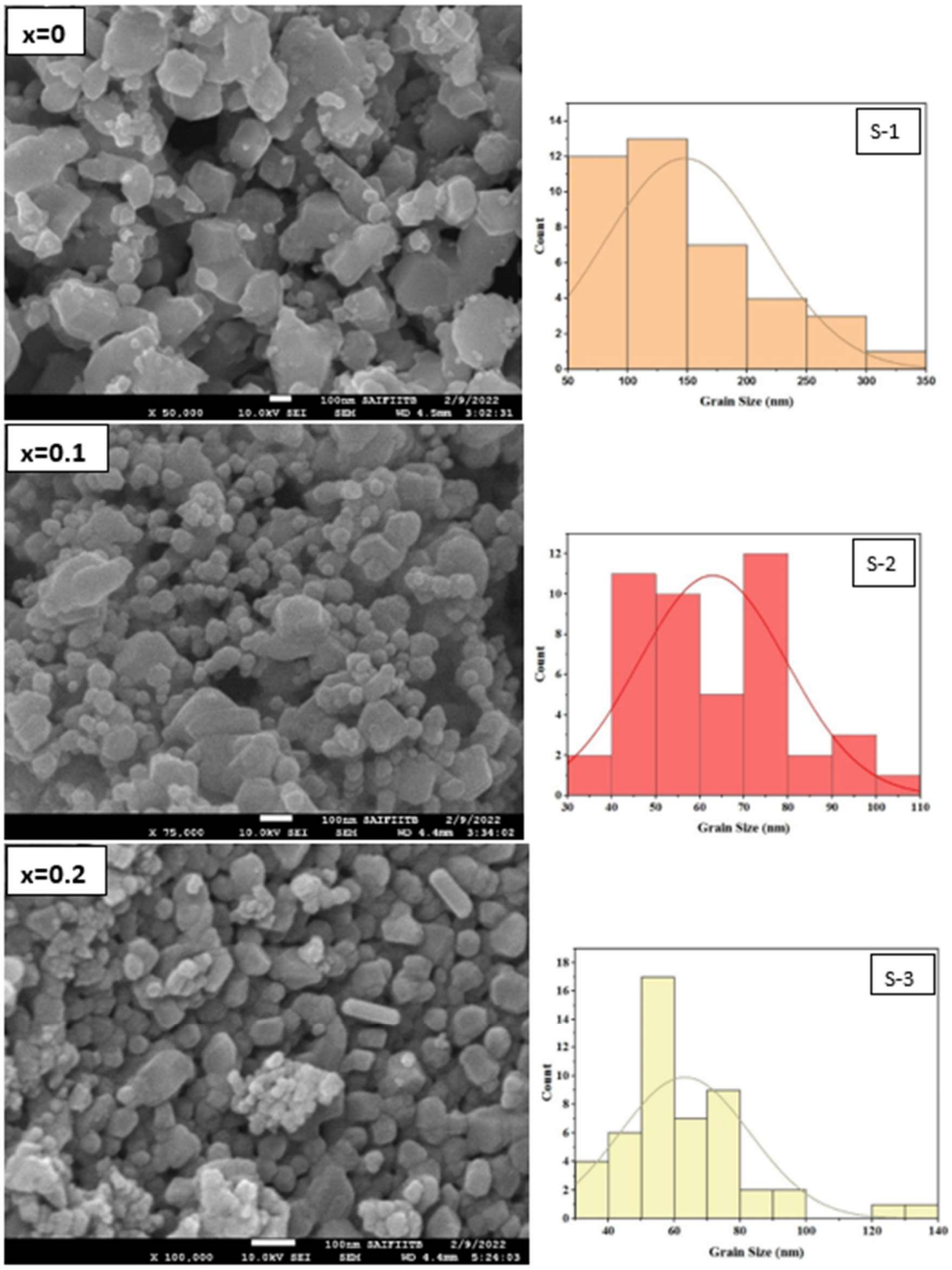

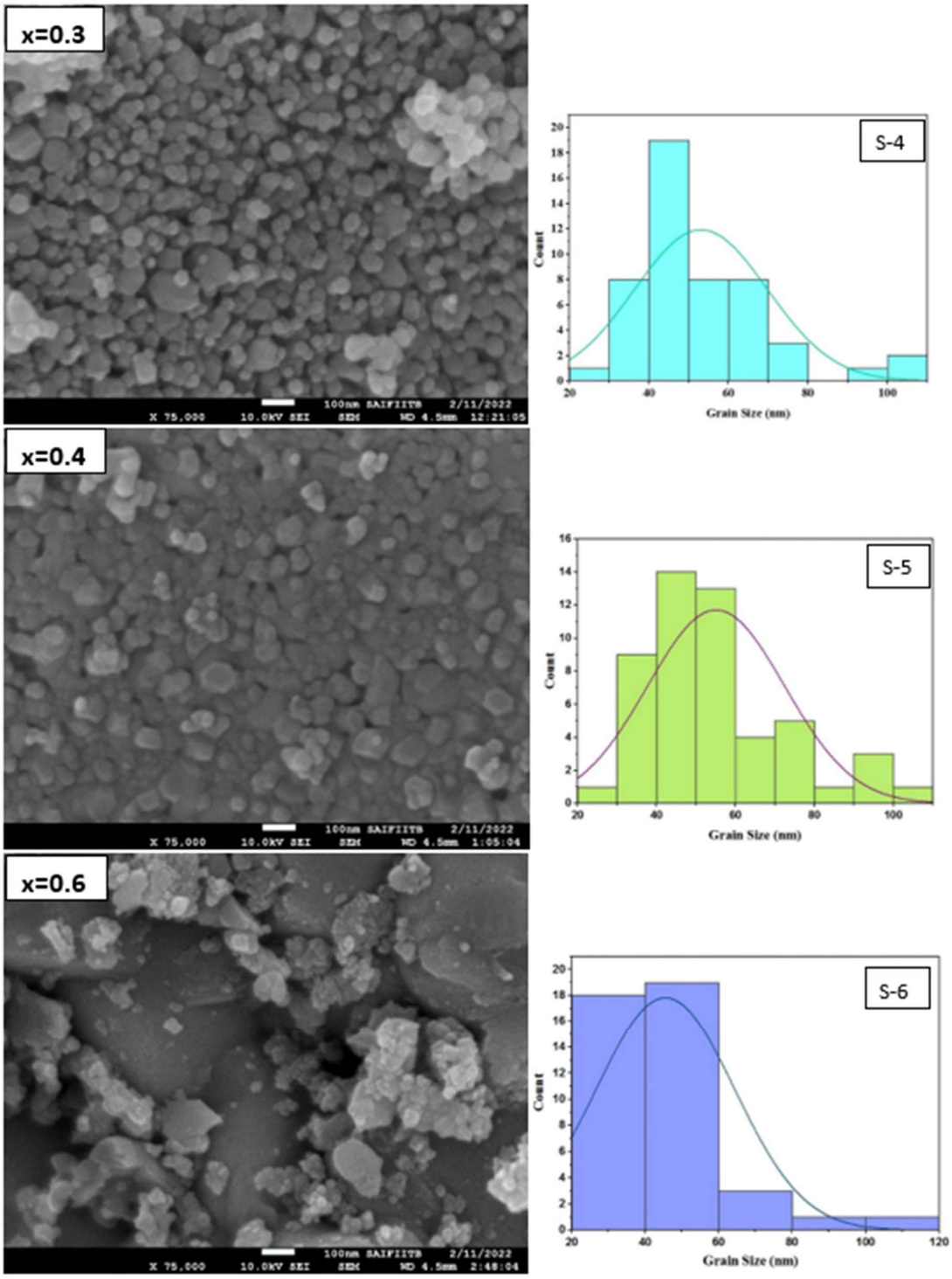

Fig. [7] SEM micrographs and histogram of (a) $Co_{0.6}Ni_{0.4}Fe_2O_4$ (b) $Co_{0.5}Ni_{0.4}Cd_{0.1}Fe_2O_4$ (c) $Co_{0.4}Ni_{0.4}Cd_{0.2}Fe_2O_4$ (d) $Co_{0.3}Ni_{0.4}Cd_{0.3}Fe_2O_4$ (e) $Co_{0.2}Ni_{0.4}Cd_{0.4}Fe_2O_4$ (f) $Co_{0.1}Ni_{0.4}Cd_{0.5}Fe_2O_4$

Table [2]: Grain Size and absorption band edges

Composition	Grain Size (nm)	Absorption Band Edges

			(Wavenumber in cm^{-1})	
	SEM	**TEM**	ν_t	ν_o
$Co_{0.6}\ Ni_{0.4}\ Fe_2\ O_4$	148	112	588.75	417.18
$Co_{0.5}\ Ni_{0.4}\ Cd_{0.1}\ Fe_2\ O_4$	62	57	597.53	420.27
$Co_{0.4}\ Ni_{0.4}\ Cd_{0.2}\ Fe_2\ O_4$	63	-	578.46	418.21
$Co_{0.3}\ Ni_{0.4}\ Cd_{0.3}\ Fe_2\ O_4$	53	48	592.42	419.80
$Co_{0.2}\ Ni_{0.4}\ Cd_{0.4}\ Fe_2\ O_4$	55	-	589.85	419.24
$Co_{0.1}\ Ni_{0.4}\ Cd_{0.5}\ Fe_2\ O_4$	46	44	574.82	418.21

The SEM micrographs and respective histogram distribution of the nanoparticles for $Co_{1-x}\ Ni_{0.4}\ Cd_x\ Fe_2\ O_4$ (where x = 0.00, 0.1, 0.2, 0.3, 0.4 and 0.5) system of ferrites are illustrated in Fig. [7]. FESEM images as in Fig. [7], further confirms the spherical shape of the ferrite nanocrystals. The average Grain size of the samples are found to be in the range 148 nm to 46 nm from their size distribution graphs in Fig. [7], which are in consistent with that obtained from HRTEM.

The crystallite size determined by XRD is different from the grain sizes observed from SEM. This indicates the grains observed in the SEM are the domains formed by aggregation of nanosize crystallites [56]. Agglomeration is the result of the magnetic interactions and high surface energy of the nanoparticles. It is observed that Grains are of well-defined boundaries and less agglomerated for doped samples as compared to pure Co-Ni Ferrite. Since the magnetization of the undoped Cobalt nickel ferrite is higher than that of the doped samples due to nonmagnetic nature of Cadmium, the dipole–dipole interaction is prevailing in undoped Cobalt-nickel ferrite nanoparticles; consequently, the attractive force between the nanoparticles of undoped sample is greater [57]. Thus agglomeration is more dominant in $Co_{0.6}\ Ni_{0.4}\ Fe_2\ O_4$ sample. The decreasing grain sizes with increase in Cd composition may be attributed to the reduction in oxygen vacancies which can be verified by the energy dispersive X-ray (EDAX) analysis of the prepared samples [58].

3.4 Transmission electron microscopy

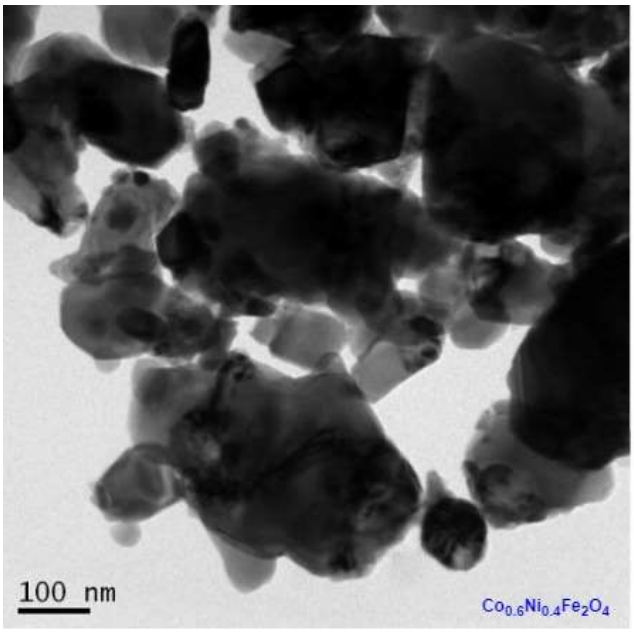
100 nm
$Co_{0.6}Ni_{0.4}Fe_2O_4$

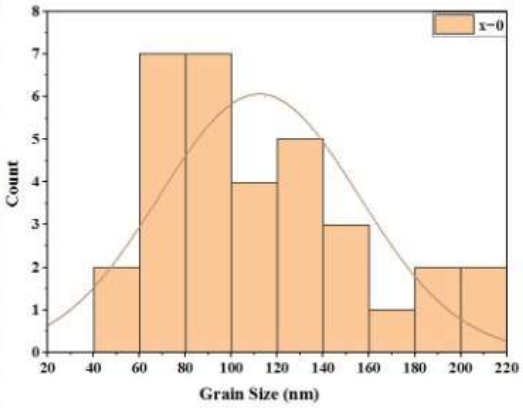
x=0
Count
Grain Size (nm)

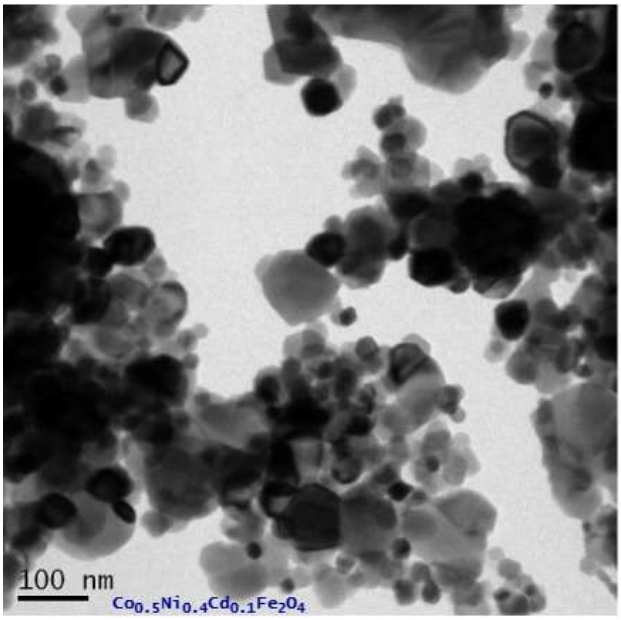
100 nm
$Co_{0.5}Ni_{0.4}Cd_{0.1}Fe_2O_4$

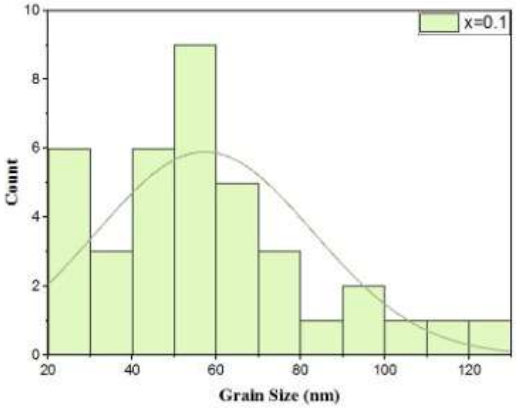
x=0.1
Count
Grain Size (nm)

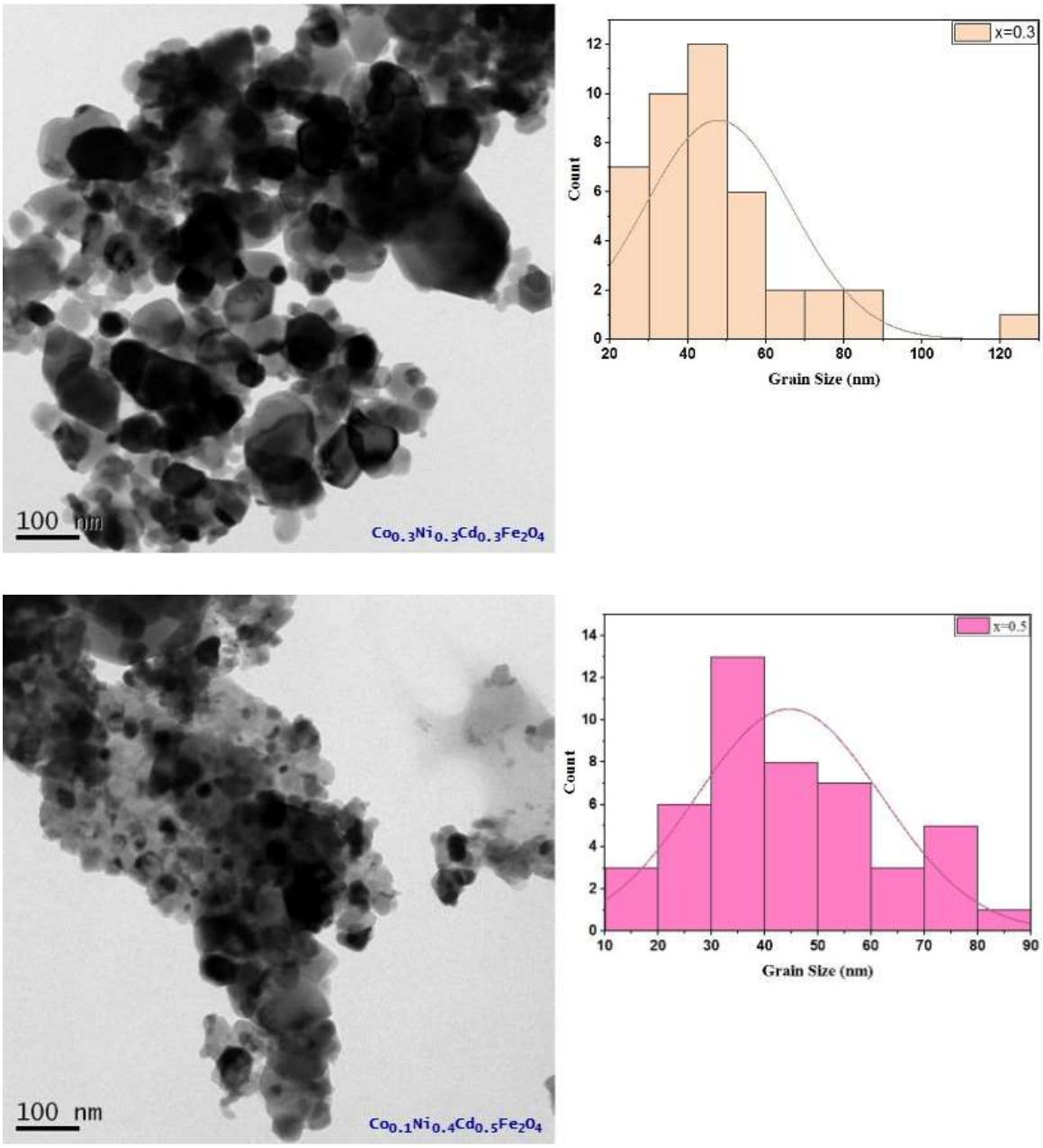

Fig. [8] TEM images and histograms of $Co_{0.6-x}$ $Ni_{0.4}$ Cd_x Fe_2 O_4 (with x=0.0, 0.1, 0.3 and 0.5)

Morphological analysis has been performed by TEM imaging technique, using a JEOL JEM-2100 TEM instrument, where gun voltage varies from 5 kV to 20 kV. TEM images show spherical morphology and uniform distribution for respective nanocrystals as in Fig. [8]. These TEM images have been analyzed by using the ImageJ software for the calculation of average Grain size, which is found as 112 nm, 57 nm, 48 nm and 44 nm for Co-Ni ferrite nanocrystals with concentration x=0, 0.1, 0.3, 0.5 respectively. The agglomerate nature of the ferrite is due to the magnetic dipole-dipole interaction among the particles [59-60]. These TEM images show that size gets decreased due to doping of Cadmium which is consistent with the XRD and SEM observations.

3.5 Magnetic Measurements

The compounds of the system $Co_{0.6-x}\ Ni_{0.4}\ Cd_x\ Fe_2\ O_4$ showed a definite hysteresis loop at room temperature, which reveals the ferrimagnetic behaviour (Figure [10]) of the system. The magnetization curve reveals the change in the magnetic behavior with Cd^{2+} substitution. From the hysteresis loops, The saturation magnetization (Ms), coercive field (Hc), and remanent magnetization (Mr), magnetic moment and remanent ratio (Mr/ Ms) of the samples can be extracted and are listed in Table [3]. These magnetic parameters depend on grain size, Cd^{2+} concentration, anisotropy and magnetic interaction of A–B sites [1, 61-63]. Apart from this, magnetic properties are strongly influenced by micro-strain that gets produced within the lattice sites due to doping as well as magnetic and non-magnetic nature of the doping elements [7]. From Table [3] it is seen that the saturation magnetization increases with increase in cadmium content upto x =0.2 and then shows decreasing trend later on.

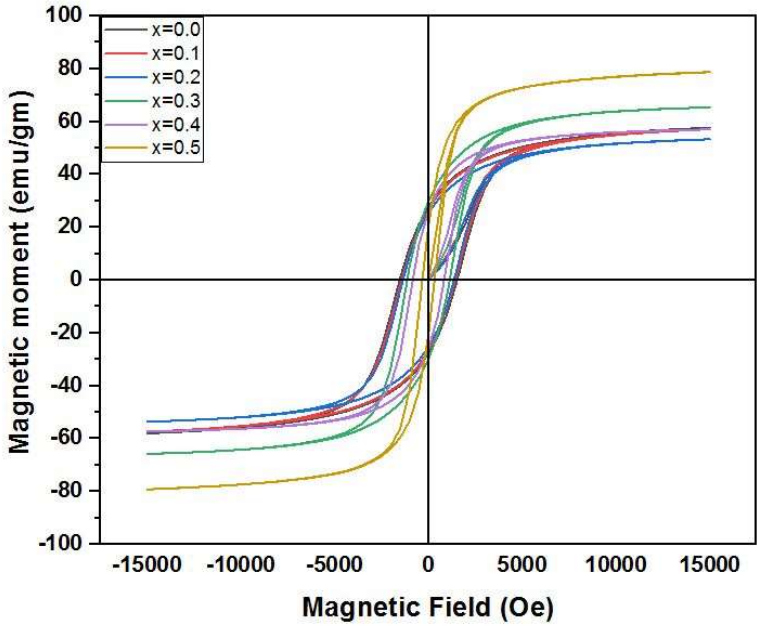

Fig. [10] M–H loops for $Co_{0.6-x}\ Ni_{0.4}\ Cd_x\ Fe_2\ O_4$ (x=0.0, 0.1, 0.2, 0.3, 0.4 and 0.5)

For ferrites, the variation in saturation magnetization Ms is attributed to both surface spin effect and cation distribution on the A and B sites. Superexchange interactions between the two magnetic cations via an intermediate oxygen ion in the spinel structure can occur as a result of intra-sublattice AA and BB interactions and inter-sublattice AB interactions. The strength of the superexchange interactions depends on the angle and distance between the two metal cations so that among them AB superexchange interaction is the strongest one and AA interaction is the weakest one and magnetic moments of two sublattices are opposite. The total magnetic moment depends on the magnetic moment of the A- and B-sites. It should be noted that the total saturation magnetization depends on several factors such as temperature, process, chemical composition, grain size, density, and so on, in addition to the distribution of cations in these two sites.

With increase in cadmium concentration Neel's two sublattice model [64] is able to explain the increase of magnetization upto $x = 0.2$ at room temperature. According to the Neel's model the resultant magnetization is the difference between A-site and B-site magnetization. The predominant super exchange interactions occurring between A and B sites

magnetic ions, favor collinear and anti-parallel alignments of the spins at A and B sites (Magnetic field effect on the complex permeability spectra in a Ni–Zn ferrite) [65]. Since the magnetic moments on A and B sites are in opposite directions eliminating each other and also the magnetization of sub-lattice B is more than that of A, the magnetization of nanoparticles is mostly caused by sub-lattice B [31]. Mathematically,

$$M_{Net} = M_A + M_B$$

where M_A and M_B are the magnetization of the sublattices A and B site, respectively. The substitutions of non-magnetic divalent cadmium ions on the A-sites transfer the trivalent iron (Fe^{3+}) ions on B sites affecting the magnetic moments of individual sub lattice and A-B interactions. As the cadmium ions increase at A site, the magnetization of tetrahedral site decreases, this results in an increase of net magnetization, which is in agreement with Neel's model [66].

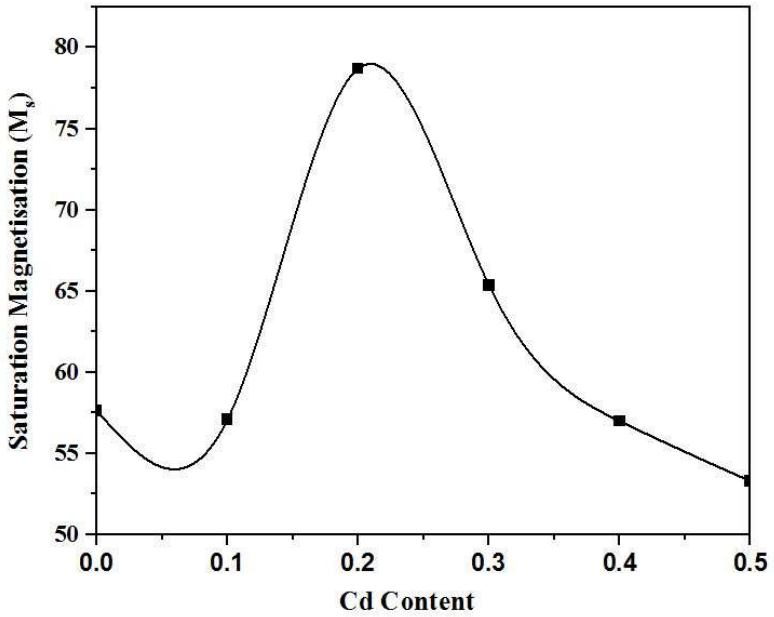

Figure [11]: Variation of Saturation Magnetisation (M_s) with Cd content

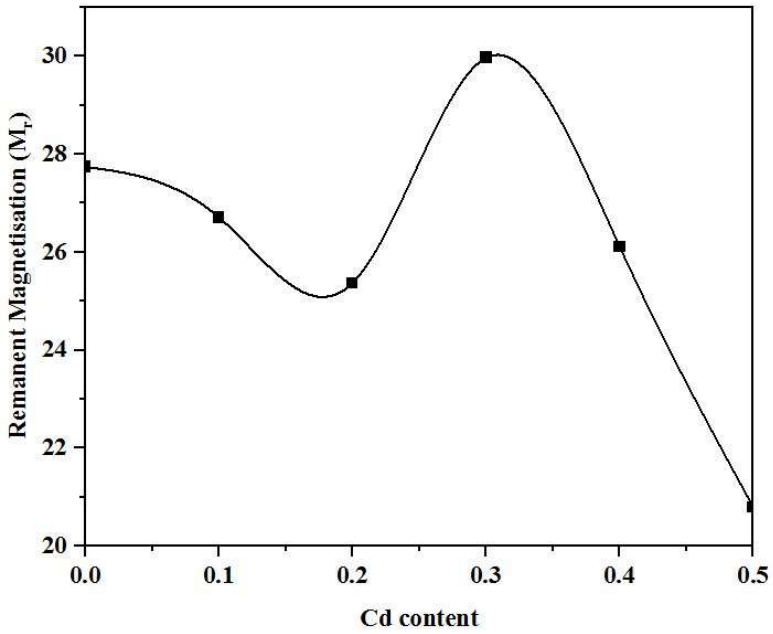

Figure [12]: Variation of Remanent Magnetisation (M_r) with Cd content

The saturation magnetization values increased from 57.64 emu/g for $Co_{0.6}Ni_{0.4}Fe_2O_4$ to reach a maximum value of 78.71 emu/g for $Co_{0.4}Ni_{0.4}Cd_{0.2}Fe_2O_4$ as indicated in Table 3, which indicates that Ms increases with increasing Cd^{2+} ions concentration until $x <= 0.2$. Similar trend was observed by other researchers too [67-69].

Substitution of diamagnetic cations in one sublattice of ferrimagnet leads to spin canting in the other sublattice resulting in decrease in total magnetization per formula unit. The reason for the decrease in magnetization beyond x=0.2 is that the magnetization of A-sublattice is so diluted that the A–B exchange interaction no longer remains stronger and thereby B–B sublattice interaction becomes strong, which in turn disturbs the parallel arrangement of spin magnetic moments on the B-site and hence canting of spin occurs. Neel's two-sublattice collinear ferrimagnetism is observed for the system up to $x \leq 0.4$ and beyond this limit three-sublattice non-collinear spin canting model is predominant. The existence of canted spin gives rise to the Yafet-Kittel angle (a Y-K), which compares the strength of A–B and B–B exchange interactions [70].

Neel's two sublattice model is unable to explain the decrease of magnetization from x =0.3 to x=0.5 at room temperature. The decrease of magnetization can be treated theoretically by triangular arrangement of spins as proposed by Yafet and Kittel (Antiferromagnetic Arrangements in Ferrites)[70]. The reason for the decrease in magnetization beyond x=0.2 is that the magnetization of A-sublattice is so diluted that the A–B exchange interaction no longer remains stronger and thereby B–B sublattice interaction becomes strong, which in turn disturbs the parallel arrangement of spin magnetic moments on the B-site and hence canting of spin occurs [71]. Therefore, in the present system the concentration dependence of Ms can be attributed to canting of spins which gives rise to Yafet-Kittel (Y-K) angles, suggesting A-B and B-B super exchange interactions to be comparable in strength. Y-K angles are computed from the data obtained in the hysteretic experiment using following equation [72]:

$$\cos \alpha_{yk} = \frac{n_B + 5(1-x)}{(7+x)}$$

where n_B is expressed in the units of Bohr-magneton and x represents the contents of cadmium. The non-zero Y–K angles suggest that the magnetization behavior cannot be described by Neel's two-sublattice model due to the presence of spin canting on B-sites, which increases the B–B interaction and consequently it weakens the A–B interaction [73]. Thus, Saturation magnetization decreases from 78.71 emu/gm ($x = 0.2$) to a minimum value of 53.29 emu/gm ($x = 0.5$) uniformly with respect to Cd concentration. This trend is in accordance with results reported by other researchers. [39, 74-77].

Table [3]: Magnetic Properties of $Co_{0.6-x}$ $Ni_{0.4}$ Cd_x Fe_2 O_4

Concentration	Saturation magnetization (Ms)	Remanance (Mr)	Coercivity (Hc)	Magnetic moment, n_B (μ_B)	Mr/Ms	Magnetic anisotropy
0	57.64	27.74	1540.75	2.43	0.4812	92510
0.1	57.08	26.71	1428.30	2.41	0.4680	84928
0.2	78.71	25.37	1356.15	3.32	0.4760	75292
0.3	65.36	29.97	1136.12	2.75	0.4585	77353
0.4	57.00	26.11	835.36	2.40	0.4580	49604
0.5	53.29	20.79	322.71	2.24	0.2641	26459

The ratio of the remanence magnetization (Mr) and saturation magnetization (Ms) i.e. $R = \mathrm{Mr}/\mathrm{Ms}$ is the key factor to conclude the magnetic nature (in the terms of single/multi domain) of the ferrite materials. [78] Thus, in the present case, the values of the remanence ratio (R = Mr /Ms) were evaluated from the M−H plots and its values are tabulated in Table [3]. As per the previous reports, if $R \geq 0.5$, then the materials consist of the single domain structure, however if $R < 0.5$, then the materials consist of the multi-domain structure [79]. As observed in Table [3], the values of R varies in between the 0.26 to 0.48, which is lesser than 0.5. It indicates the existence of multi-domain particles in the prepared samples. In the multi-domain magnetic structure, the movements of the domain walls permits trouble-free alteration in the orientations via externally applied magnetics field [73] [80-83].

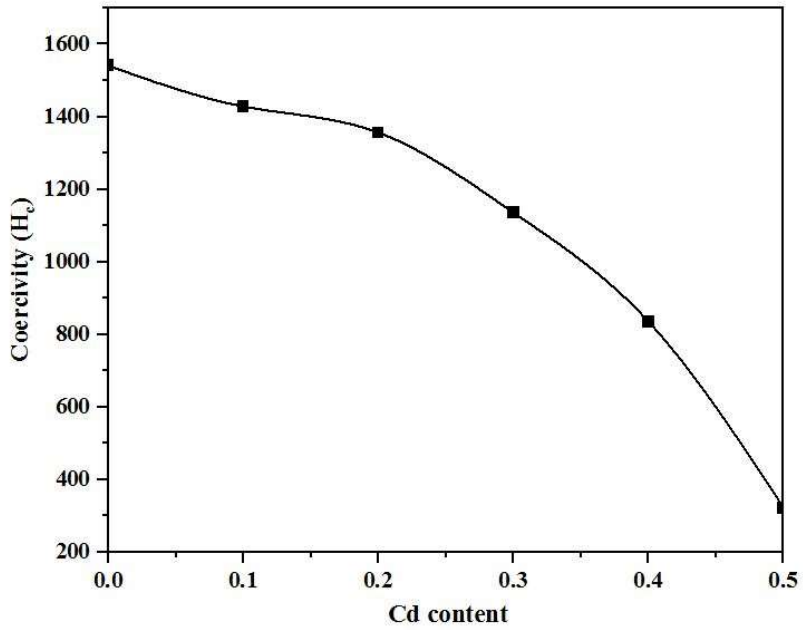

Figure [13]: Variation of Coercivity (Hc) with Cd content

The Hc values given in Table [3] show a uniform decline with increasing the Cd substitution. This value refers to the intensity of the magnetic field required to reduce the magnetization of the magnetic sample to zero after the magnetization of the sample has reached saturation (Cation distribution investigation and characterizations of Ni1−xCdxFe2O4 nanoparticles synthesized by citrate gel process) [84]. In general, the Hc is a function of anisotropy energy ($K_{ef}V$); in fact, the more anisotropy energy is, the more and more the Hc is. Generally, the value of $K_{ef}V$ is written as follows [85]:

$$K_{ef}V = E_{shape} + E_{surface} + E_{ME} + E_{MC}$$

where the anisotropy E_{shape} is related to the particle shape. Since the shape of the nanoparticles studied is independent of increasing the Cd substitution, so this energy does not have significant effects on Hc changes. $E_{surface}$ term is associated with surface anisotropy. The smaller the particle sizes of the nanoparticles, the higher the surface area of the nanoparticles and hence greater the anisotropy factor of the nanoparticles. E_{ME} is related to the magnetoelastic anisotropy, which in fact the lattice parameter shrinkage causes the magnetic atoms to close together, resulting in a coupling between the spins and the lattice followed by the increase of the E_{ME} contribution. E_{MC} is linked to magnetic anisotropy energy. This energy is proportional to the anisotropy constant K_1 as given in Table [3]. Because of this anisotropy, the magnetic material will be directed in the direction where it can be easily magnetized. Finally, the non-monotonic Hc behavior observed for the samples is a superposition of the changes in the three terms of the anisotropy energy of $E_{surface}$, E_{ME} and E_{MC} in the studied nanoparticles.

Fig. [13] demonstrate the coercivity as a function of Cadmium concentration. For Co-Ni Ferrite (at $x = 0$), the higher values of coercivity Hc value indicates the significant value of magnitude of magneto-crystalline anisotropy for the sample. As cobalt is a hard magnetic material, its high magneto crystalline nature improves the value of coercivity. The magneto-crystalline anisotropy originates from spin-orbit (L-S) coupling i.e. interactions of orbital

magnetic moments with spin magnetic moments. The strong L-S coupling determines large magnitude of magneto-crystalline anisotropy [86] and for Co-Ni Ferrite; it only originates from the existence of Co^{2+} ions at octahedral B sites [87]. A decrease in coercivity with increasing Cadmium concentration may be attributed to the lower magnetocrystalline anisotropy of Cd^{2+} as compared to that of Co^{2+} ions which in turn decreases the domain wall energy. That leads to lower coercivity according to the Stoner Wolfforth model for nanoparticles ($H_C \sim 2K/M_S$) [88-91, 57].

Magnetocrystalline anisotropy is the energy necessary to deflect the magnetic moment in a single crystal from the easy to the hard direction. Easy axis is the direction inside a crystal, along which small applied magnetic field is sufficient to reach the saturation magnetization. Hard axis is the direction inside a crystal, along which large applied magnetic field is needed to reach the saturation magnetization. The easy and hard directions arise from the interaction of the spin magnetic moment with the crystal lattice (spin-orbit coupling). Magnetic anisotropy strongly affects the shape of hysteresis loops and controls the coercivity and remanence. Anisotropy is also of considerable practical importance because it is exploited in the design of most magnetic materials of commercial importance. [92]

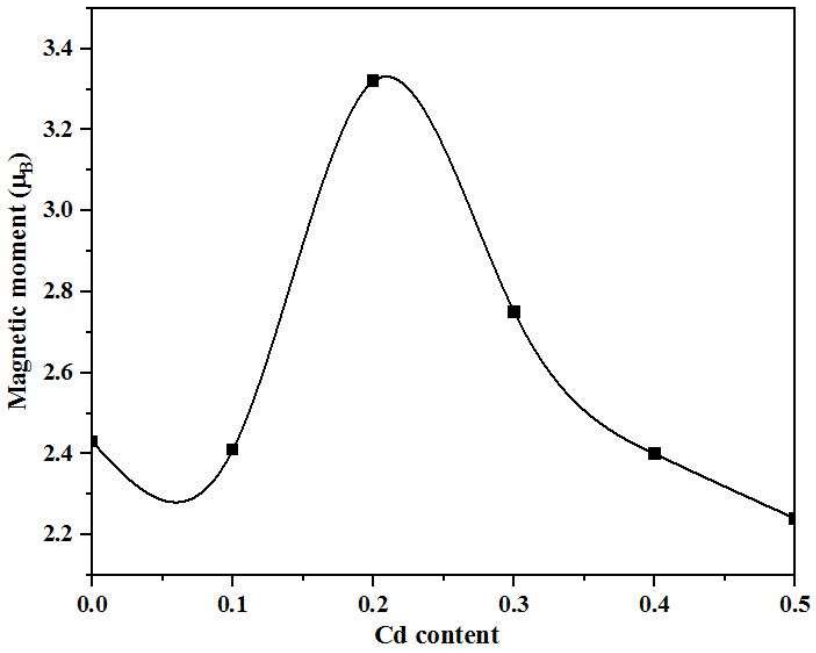

Fig. [14] Variation of Magnetic Moment (n_B) with Cd content.

The values of magnetic moment can be obtained using the values of saturation magnetization (M_s) and molecular weight of the samples from the relation [93],

$$n_B = \left(M_s \times \frac{Mol.Wt.}{5585}\right) \text{ emu/g.}$$

Studies had shown that Co^{2+} ions preferentially reside in the B-site [94] which is consistent with their favor for large octahedral site energy. The non-magnetic Cd^{2+} ions with the large ionic radius prefer to occupy for the tetrahedral site (A-site) [95] [92], replacing the Fe^{3+} magnetic ions. Fe^{3+} occupies both A and B-site. Since Cd^{2+} ions had no magnetic moment, the fraction of magnetic moment of A-site was reduced and the net magnetic moment of B-site was increased. As a result, the net magnetic moment was improved with increasing Cd

concentration. [57]. This Neel's two sublattice model [64] explains the increase of magnetic moment upto $x \leq 0.2$ with respect to Cadmium content. The total magnetic moment is increased from 2.43 μ_B for $x = 0$ to 3.32 μ_B for $x = 0.2$ [96]. The reason for the decrease of magnetization beyond x = 0.2 is that the magnetization of A-sublattice is diluted so much that the A–B lattice interaction remains no longer stronger and so B–B sublattice interaction becomes strong, which in turn disrupts the parallel arrangement of spin magnetic moments on the B-site and hence canting of spin occurs [77]. That deviation from collinear ferrimagnetism led magnetic moment to decrease from 2.75 μ_B ($x = 0.3$) to 2.24 ($x = 0.5$) [97].

4. Conclusion

Structural, morphological and magnetic properties of Cadmium substituted nanocrystalline cobalt ferrite, synthesized by the sol-gel auto-combustion method, has been investigated in the present study. All samples confirms the formation of cubic spinel structure with a *Fd-3m* space group. It is observed that the lattice constant, bulk density and XRD density increases while the average crystallite size and porosity decrease with the Cd^{2+} concentration. The crystallite size of the sample lies in the range 20.33 to 31.38 nm. Lattice constant values are found to be in the range 8.3719 Å to 8.4742 Å. The variation in the lattice parameter indicates that the system under study conform the Vegard's law. From FTIR study, the characteristic bands ν_1 and ν_2 were found to be located within the ranges 574–597 and 417–420 cm^{-1}, owing to the fundamental vibrational mode of tetrahedral (A) and octahedral (B) position of ferrites. The SEM micrographs for $Co_{1-x}Ni_{0.4}Cd_xFe_2O_4$ (where x = 0.00, 0.1, 0.2, 0.3, 0.4 and 0.5) ferrite confirms the spherical morphology of the ferrite nanocrystals having the average Grain size in the range of 148 nm to 46 nm. HR-TEM predicts the grain size in the range of 112-44 nm. Magnetic studies reveal the saturation magnetization (M_s), Remanent magnetization (M_r) are observed to be increasing upto $x = 0.2$ concentration of Cd and decreasing thereafter due to spin canting effect. The maximum saturation magnetization (Ms) was found to be 78 emu/gm for the sample with x = 0.2. Total magnetic moment (n_B) follow the similar trend as M_s. Coercivity of all samples is reducing linearly with increasing Cd concentration. A decrease in coercivity with increasing Cadmium concentration may be attributed to the lower magnetocrystalline anisotropy of Cd^{2+} as compared to that of Co^{2+} ions which in turn decreases the domain wall energy. Remanence ratio (R<0.5) indicates the existence of multi-domain particles in the prepared samples. The substitution of Cd^{2+} plays an important role to modify the structural and magnetic properties of Co-Ni ferrites.

References:

1. Rimi Sharma, Sonal Singhal, Structural, magnetic and electrical properties of zinc doped nickel ferrite and their application in photo catalytic degradation of methylene blue, Physica B: Condensed Matter, Volume 414, 2013, Pages 83-90, ISSN 0921-4526, https://doi.org/10.1016/j.physb.2013.01.015.
2. Asiri, S., Sertkol, M., Guner, S., Gungunes, H., Batoo, K. M., Saleh, T. A., Baykal, A. (2018). Hydrothermal synthesis of CoyZnyMn1-2yFe2O4 nanoferrites: Magneto optical investigation. CERAMICS INTERNATIONAL, 44(5), 5751–5759. doi:10.1016/j.ceramint.2017.12.233

3. Silambarasu, A., Manikandan, A. & Balakrishnan, K. Room-Temperature Superparamagnetism and Enhanced Photocatalytic Activity of Magnetically Reusable Spinel ZnFe2O4 Nanocatalysts. J Supercond Nov Magn 30, 2631–2640 (2017). https://doi.org/10.1007/s10948-017-4061-1
4. Mathubala, G., Manikandan, A., Arul Antony, S., & Ramar, P. (2016). Enhanced photocatalytic activity of spinel Cu x Mn1–x Fe2O4 nanocatalysts for the degradation of methylene blue dye and opto-magnetic properties. Nanoscience and Nanotechnology Letters, 8(5), 375-381.
5. A.M. Shahare, D.S. Choudhary, A.V. Bagde, Y.S. Bopche, Influence of Cr3+ on structural and dielectric properties of Ni0.25Cu0.2Zn0.55Fe2O4 nanoparticles, Materials Today: Proceedings, Volume 29, Part 3, 2020, Pages 839-843, ISSN 2214-7853, https://doi.org/10.1016/j.matpr.2020.04.879.
6. Jun Xiang, Yanqiu Chu, Xionghui Zhang, Xiangqian Shen, Magnetic and microwave absorption properties of electrospun Co0.5Ni0.5Fe2O4 nanofibers, Applied Surface Science, Volume 263, 2012, Pages 320-325, ISSN 0169-4332, https://doi.org/10.1016/j.apsusc.2012.09.052.
7. Rajnish Kumar, Manoranjan Kar, Lattice strain induced magnetism in substituted nanocrystalline cobalt ferrite, Journal of Magnetism and Magnetic Materials, Volume 416, 2016, Pages 335-341, ISSN 0304-8853, https://doi.org/10.1016/j.jmmm.2016.05.035.
8. R.C. Kambale, P.A. Shaikh, S.S. Kamble, Y.D. Kolekar, Effect of cobalt substitution on structural, magnetic and electric properties of nickel ferrite, Journal of Alloys and Compounds, Volume 478, Issues 1–2, 2009, Pages 599-603, ISSN 0925-8388, https://doi.org/10.1016/j.jallcom.2008.11.101.
9. Zhang, J., Fu, J., Tan, G., Li, F., Luo, C., Zhao, J., Peng, Y. (2012). Nanoscale characterization and magnetic reversal mechanism investigation of electrospun NiFe2O4 multi-particle-chain nanofibres. Nanoscale, 4(8), 2754. https://doi.org/10.1039/C2NR00024E
10. S. Chakrabarty, A. Dutta, M. Pal, Enhanced magnetic properties of doped cobalt ferrite nanoparticles by virtue of cation distribution, Journal of Alloys and Compounds, Volume 625, 2015, Pages 216-223, ISSN 0925-8388, https://doi.org/10.1016/j.jallcom.2014.10.179.
11. M.M. Mallapur, P.A. Shaikh, R.C. Kambale, H.V. Jamadar, P.U. Mahamuni, B.K. Chougule, Structural and electrical properties of nanocrystalline cobalt substituted nickel zinc ferrite, Journal of Alloys and Compounds, Volume 479, Issues 1–2, 2009, Pages 797-802, ISSN 0925-8388, https://doi.org/10.1016/j.jallcom.2009.01.142.
12. Ashwini Kumar, Poorva Sharma, Dinesh Varshney, Structural, vibrational and dielectric study of Ni doped spinel Co ferrites: Co1−xNixFe2O4 (x=0.0, 0.5, 1.0), Ceramics International, Volume 40, Issue 8, Part B, 2014, Pages 12855-1286, ISSN 0272-8842, https://doi.org/10.1016/j.ceramint.2014.04.140.
13. Pragati Jadhav, Ketaki Patankar, Vikas Mathe, N.L. Tarwal, Jae-Hung Jang, Vijaya Puri, Structural and magnetic properties of Ni0.8Co0.2−2xCuxMnxFe2O4 spinel ferrites prepared via solution combustion route, Journal of Magnetism and Magnetic

Materials, Volume 385, 2015, Pages 160-165, ISSN 0304-8853, https://doi.org/10.1016/j.jmmm.2015.03.020.

14. Ashok Kumar, Nisha Yadav, Dinesh S. Rana, Parmod Kumar, Manju Arora, R.P. Pant, Structural and magnetic studies of the nickel doped CoFe2O4 ferrite nanoparticles synthesized by the chemical co-precipitation method, Journal of Magnetism and Magnetic Materials, Volume 394, 2015, Pages 379-384, ISSN 0304-8853, https://doi.org/10.1016/j.jmmm.2015.06.087.
15. Hosseini, S.A., Niaei, A., Salari, D. and Aghazadeh, F. (2010), Nanostructure Copper-exchanged ZSM-5 Catalytic Activity for Conversion of Volatile Organic Compounds (Toluene and Ethyl Acetate). Chin. J. Chem., 28: 143-148. https://doi.org/10.1002/cjoc.201090045
16. Santosh Bhukal, S. Bansal, Sonal Singhal, Co0.6Zn0.4Cu0.2CdxFe1.8−xO4 (0.2⩽x⩽0.8) magnetic ferrite nano-particle: Synthesis, characterization and photo-catalytic degradation of methyl orange, Journal of Molecular Structure, Volume 1059, 2014, Pages 150-158, ISSN 0022-2860, https://doi.org/10.1016/j.molstruc.2013.11.036.
17. SINGHAL, S., JAUHAR, S., CHANDRA, K. et al. Spin canting phenomenon in cadmium doped cobalt ferrites, CoCd x Fe2−x O 4 (x = 0·0, 0·2, 0·4, 0·6, 0·8 and 1·0), synthesized using sol–gel auto combustion method. Bull Mater Sci 36, 107–114 (2013). https://doi.org/10.1007/s12034-013-0439-2
18. B.D. Cullity, J.W. Weymouth, Elements of X-ray diffraction, Am. J. Phys. 25 (6) (1957) 394–395.
19. Beyranvand, Morteza; Gholizadeh, Ahmad (2020). Structural, magnetic, elastic, and dielectric properties of Mn0.3-xCdxCu0.2Zn0.5Fe2O4 nanoparticles. Journal of Materials Science: Materials in Electronics, doi:10.1007/s10854-020-03073-8
20. Gharibshahian, M., Nourbakhsh, M.S. & Mirzaee, O. Evaluation of the superparamagnetic and biological properties of microwave assisted synthesized Zn & Cd doped CoFe2O4 nanoparticles via Pechini sol–gel method. J Sol-Gel Sci Technol 85, 684–692 (2018). https://doi.org/10.1007/s10971-017-4570-1
21. Noor, S., Rahman, M. M., Sikder, S. S., & Hakim, M. A. (2011). Effect of Cd substitution on structural and transport properties of Co-ferrites. Jahangirnagar Univ J Sci, 34, 1-11.
22. Kale, C.M. & More, S & Babrekar, Mahesh & Shukla, S. (2018). Enhancement in Physical Properties of Cd Substituted Copper ferrite. World Journal of Pharmaceutical Research. 7. 491-505. 10.20959/wjpr201812-12526.
23. DALAWAI, S.P., SHINDE, T.J., GADKARI, A.B. et al. Structural properties of Cd–Co ferrites. Bull Mater Sci 36, 919–922 (2013). https://doi.org/10.1007/s12034-013-0529-1
24. R.G. Kharabe, R.S. Devan, B.K. Chougale, Structural and electrical properties of Cd-substituted Li–Ni ferrites, Journal of Alloys and Compounds, Volume 463, Issues 1–2, 2008, Pages 67-72, ISSN 0925-8388, https://doi.org/10.1016/j.jallcom.2007.09.061.
25. R. Zahir, F.-U.-Z Chowdhury, M.M. Uddin, M.A. Hakim, Structural, magnetic and electrical characterization of Cd-substituted Mg ferrites synthesized by double sintering

technique, Journal of Magnetism and Magnetic Materials, Volume 410, 2016, Pages 55-62, ISSN 0304-8853, https://doi.org/10.1016/j.jmmm.2016.03.019.

26. Patange, S.M., Shirsath, S.E., Jadhav, S.S. and Jadhav, K.M. (2012), Cation distribution study of nanocrystalline NiFe2−xCrxO4 ferrite by XRD, magnetization and Mössbauer spectroscopy. Phys. Status Solidi A, 209: 347-352. https://doi.org/10.1002/pssa.201127232
27. Mona Mouallem-Bahout, Sarah Bertrand, Octavio Peña, Synthesis and characterization of Zn1−xNixFe2O4 spinels prepared by a citrate precursor, Journal of Solid State Chemistry, Volume 178, Issue 4, 2005, Pages 1080-1086, ISSN 0022-4596, https://doi.org/10.1016/j.jssc.2005.01.009.
28. B.D. Cullity, Elements of X-ray diffraction (Addison Wesley Pub. Co. Inc., London, 1956), p. 99
29. R.F. Strickland-Constable, Kinetics and Mechanism of Crystallization, Academic Press, New York, 1968.
30. Wahsh, M.M.S. & Othman, Atef & Awad, Kamal & Girgis, E. & Mabrouk, Mohamed & Morsy, Fatma. (2019). Synthesis and magneto-optical properties of cobalt ferrite/silica nanoparticles doped with Cd2+ ions. Main Group Chemistry. 18. 397-410. 10.3233/MGC-180769.
31. Ch. Venkata Reddy, Chan Byon, B. Narendra, D. Baskar, G. Srinivas, Jaesool Shim, S.V. Prabhakar Vattikuti, Investigation of structural, thermal and magnetic properties of cadmium substituted cobalt ferrite nanoparticles, Superlattices and Microstructures, Volume 82, 2015, Pages 165-173, ISSN 0749-6036, https://doi.org/10.1016/j.spmi.2015.02.014.
32. Radheshyam Rai, Kavita Verma, Seema Sharma, Swapna S. Nair, Manuel Almeida Valente, Andrei L. Kholkin, Nikolai A. Sobolev, Structure and magnetic properties of Cd doped copper ferrite, Journal of Alloys and Compounds, Volume 509, Issue 28, 2011, Pages 7585-7590, ISSN 0925-8388, https://doi.org/10.1016/j.jallcom.2011.04.045.
33. Patil, M.R., Rendale, M.K., Mathad, S.N. et al. FTIR spectra and elastic properties of Cd-substituted Ni–Zn ferrites. Int. J Self-Propag. High-Temp. Synth. 26, 33–39 (2017). https://doi.org/10.3103/S1061386217010083
34. Patil, S.A., Mahajan, V.C., Ghatage, A.K., & Lotke, S.D. (1998). Structure and magnetic properties of Cd and Ti/Si substituted cobalt ferrites. Materials Chemistry and Physics, 57, 86-91. https://doi.org/10.1016/S0254-0584(98)00202-8
35. S. Akhter, D. P. Paul, M. A. Hakim, D. K. Saha, and S. M. Hoque , "Microstructure And Electromagnetic Properties Of Li-Cd Ferrites", AIP Conference Proceedings 1347, 244-247 (2011) https://doi.org/10.1063/1.3601827
36. B.D. Cullity, S.R Stock, Elements of X-Ray Diffraction, 3rd Edition, Prentice Hall, 2001.
37. J. Li, Y. Yang, G. Wang, L. Guo, Y. Rao, G. Gan, H. Zhang, Enhanced structure and microwave magnetic properties of MgZn ferrite by Cd $^{2+}$ ion substitution for LTCC applications, Ceramics International (2019), doi: https://doi.org/10.1016/j.ceramint.2019.11.146.

38. Talat Zeeshan, Safia Anjum, Salma Waseem, Madeeha Riaz, Rehana Zia, Structural, optical, magnetic and (Y–K) angle studies of CdxCo1-xCr0.5Fe1.5O4 ferrite, Ceramics International, Volume 46, Issue 3, 2020, Pages 3935-3943, ISSN 0272-8842, https://doi.org/10.1016/j.ceramint.2019.10.122.
39. B.R. Karche, B.V. Khasbardar, A.S. Vaingankar, X-ray, SEM and magnetic properties of MgCd ferrites, Journal of Magnetism and Magnetic Materials, Volume 168, Issue 3, 1997, Pages 292-298, ISSN 0304-8853, https://doi.org/10.1016/S0304-8853(96)00705-6.
40. K.J. Standley, Oxide magnetic materials (Oxford at Clarendon press, London, 1962), p. 24
41. A.M. El-Sayed (2002). Effect of chromium substitutions on some properties of NiZn ferrites. , 28(6), 651–655. doi:10.1016/s0272-8842(02)00022-6
42. B Muhammad Ajmal, Asghari Maqsood, Structural, electrical and magnetic properties of Cu1−xZnxFe2O4 ferrites (0≤x≤1), Journal of Alloys and Compounds, Volume 460, Issues 1–2, 2008, Pages 54-59, ISSN 0925-8388, https://doi.org/10.1016/j.jallcom.2007.06.019.
43. Santosh S. Jadhav, Sagar E. Shirsath, Sunil M. Patange, and K. M. Jadhav , "Effect of Zn substitution on magnetic properties of nanocrystalline cobalt ferrite", Journal of Applied Physics 108, 093920 (2010) https://doi.org/10.1063/1. 3499346.
44. Modi, K.B. Elastic moduli determination through IR spectroscopy for zinc substituted copper ferri chromates. Journal of Materials Science 39, 2887–2890 (2004). https://doi.org/10.1023/B:JMSC.0000021472.00590.9b
45. Waldron, R.D. (1955) Infrared Spectra of Ferrites. Physical Review, 99, 1727-1735. https://doi.org/10.1103/PhysRev.99.1727
46. D Ravinder, Far-infrared spectral studies of mixed lithium–zinc ferrites, Materials Letters, Volume 40, Issue 5, 1999, Pages 205-208, ISSN 0167-577X, https://doi.org/10.1016/S0167-577X(99)00075-0.
47. Ladgaonkar, B.P., Kolekar, C.B. & Vaingankar, A.S. Infrared absorption spectroscopic study of Nd3+ substituted Zn-Mg ferrites. Bull Mater Sci 25, 351–354 (2002). https://doi.org/10.1007/BF02704131.
48. Ahmad Gholizadeh, A comparative study of the physical properties of Cu-Zn ferrites annealed under different atmospheres and temperatures: Magnetic enhancement of Cu0.5Zn0.5Fe2O4 nanoparticles by a reducing atmosphere, Journal of Magnetism and Magnetic Materials, Volume 452, 2018, Pages 389-397, ISSN 0304-8853, https://doi.org/10.1016/j.jmmm.2017.12.109.
49. N. Gandhi, K. Singh, A. Ohlan, D.P. Singh, S.K. Dhawan, Thermal, dielectric and microwave absorption properties of polyaniline–CoFe2O4 nanocomposites, Compos. Sci. Technol. 71 (2011) 1754–1760, https://doi.org/10.1016/j.compscitech.2011.08.010.
50. Rendale, M.K., Mathad, S.N., and Puri, V., Thick films of magnesium zinc ferrite with lithium substitution: Structural characteristics, Int. J. Self-Propag. High-Temp. Synth., 2015, vol. 24, no. 2, pp. 78–84. doi 10.3103/S1061386215020053.

51. Modi, K.B., Rangolia, M.K., Chhantbar, M.C., and Joshi, H.H., Study of infrared spectroscopy and elastic properties of fine and coarse grained nickel–cadmium ferrites, J. Mater. Sci., 2006, vol. 41, no. 22, pp. 7308–7318. doi 10.1007/s10853-006-0929-3.
52. T. Shanmugavel, S. Gokul Raj, G. Ramesh Kumar, G. Rajarajan, D. Saravanan, Cost effective preparation and characterization of nanocrystalline nickel ferrites (NiFe2O4) in low temperature regime, Journal of King Saud University - Science, Volume 27, Issue 2, 2015, Pages 176-181, ISSN 1018-3647, https://doi.org/10.1016/j.jksus.2014.12.006.
53. GRIMES, N., COLLETT, A. Infrared Absorption Spectra of Ferrites. Nature Physical Science 230, 158 (1971). https://doi.org/10.1038/physci230158a0
54. Nejati, K., Zabihi, R. Preparation and magnetic properties of nano size nickel ferrite particles using hydrothermal method. Chemistry Central Journal 6, 23 (2012). https://doi.org/10.1186/1752-153X-6-23
55. De, Manojit & Mukherjee, Aniruddha & Tewari, H.. (2015). Characterization of cadmium substituted nickel ferrites prepared using auto-combustion technique. Processing and Application of Ceramics. 9. 193-197. 10.2298/PAC1504193D.
56. T. Aswani, V. Pushpa Manjari, B. Babu, Sk. Muntaz Begum, G. Rama Sundari, K. Ravindranadh, R.V.S.S.N. Ravikumar, Spectral characterizations of undoped and Cu2+doped CdO nanopowder, Journal of Molecular Structure, Volume 1063, 2014, Pages 178-183, ISSN 0022-2860, https://doi.org/10.1016/j.molstruc.2014.01.059.
57. M. Rahimi, M. Eshraghi, P. Kameli, Structural and magnetic characterizations of Cd substituted nickel ferrite nanoparticles, Ceramics International, Volume 40, Issue 10, Part A, 2014, Pages 15569-15575, ISSN 0272-8842, https://doi.org/10.1016/j.ceramint.2014.07.033.
58. Hemant Singh, K.L. Yadav, Structural, dielectric, vibrational and magnetic properties of Sm doped BiFeO3 multiferroic ceramics prepared by a rapid liquid phase sintering method, Ceramics International, Volume 41, Issue 8, 2015, Pages 9285-9295, ISSN 0272-8842, https://doi.org/10.1016/j.ceramint.2015.03.212.
59. S.T. Alone, Sagar E. Shirsath, R.H. Kadam, K.M. Jadhav, Chemical synthesis, structural and magnetic properties of nano-structured Co–Zn–Fe–Cr ferrite, Journal of Alloys and Compounds, Volume 509, Issue 16, 2011, Pages 5055-5060, ISSN 0925-8388, https://doi.org/10.1016/j.jallcom.2011.02.006.
60. Monika Saini, Rajni Shukla, Ashok Kumar, Cd2+ substituted nickel ferrite doped polyaniline nanocomposites as effective shield against electromagnetic radiation in X-band frequency, Journal of Magnetism and Magnetic Materials, Volume 491, 2019, 165549, ISSN 0304-8853, https://doi.org/10.1016/j.jmmm.2019.165549.
61. N.M. Deraz, M.M. Hessien, Structural and magnetic properties of pure and doped nanocrystalline cadmium ferrite, Journal of Alloys and Compounds, Volume 475, Issues 1–2, 2009, Pages 832-839, ISSN 0925-8388, https://doi.org/10.1016/j.jallcom.2008.08.034.
62. Asima Anwar, Sonia Zulfiqar, Muhammad Asif Yousuf, Sameh A. Ragab, Muhammad Azhar Khan, Imran Shakir, Muhammad Farooq Warsi, Impact of rare earth Dy+3 cations on the various parameters of nanocrystalline nickel spinel ferrite, Journal of

Materials Research and Technology, Volume 9, Issue 3, 2020, Pages 5313-5325, ISSN 2238-7854, https://doi.org/10.1016/j.jmrt.2020.03.057.

63. Naaz, F., Dubey, H.K., Kumari, C. et al. Structural and magnetic properties of MgFe2O4 nanopowder synthesized via co-precipitation route. SN Appl. Sci. 2, 808 (2020). https://doi.org/10.1007/s42452-020-2611-9
64. Neel, L. (1948) Annales de Physique, 3, 137-198.
65. T. Tsutaoka, T. Nakamura, K. Hatakeyama, "Magnetic field effect on the complex permeability spectra in a Ni–Zn ferrite", Journal of Applied Physics 82, 3068-3071 (1997) https://doi.org/10.1063/1.366145.
66. P. B. Belavi, G. N. Chavan, B. K. Bammannavar, L. R. Naik, and R. K. Kotnala , "Magnetic Properties of Cd Substituted Ni-Cu Ferrites", AIP Conference Proceedings 1349, 1249-1250 (2011) https://doi.org/10.1063/1.3606319.
67. Sonal Singhal, Sheenu Jauhar, N. Lakshmi, S. Bansal, Mn^{3+} substituted Co–Cd ferrites, $CoCd_{0.4}Mn_xFe_{1.6-x}O_4$ ($0.1 \leqslant x \leqslant 0.6$): Cation distribution, structural, magnetic and electrical properties, Journal of Molecular Structure, Volume 1038, 2013, Pages 45-51, ISSN 0022-2860, https://doi.org/10.1016/j.molstruc.2013.01.020.
68. T.T. Srinivasan, R. Ravandranathan, L.E. Cross, R. Newham, S.G. Sanker, K.C. Patil, , "Studies on high-density nickel zinc ferrite and its magnetic properties using novel hydrazine precursors", Journal of Applied Physics 63, 3789-3791 (1988) https://doi.org/10.1063/1.340615.
69. M. Manjurul Haque, M. Huq, M.A. Hakim, Densification, magnetic and dielectric behaviour of Cu-substituted Mg–Zn ferrites, Materials Chemistry and Physics, Volume 112, Issue 2, 2008, Pages 580-586, ISSN 0254-0584, https://doi.org/10.1016/j.matchemphys.2008.05.097.
70. Yafet, Y., & Kittel, C. (1952). Antiferromagnetic arrangements in ferrites. Physical Review, 87(2), 290.
71. Patton, C. E., & Liu, Y. H. (1983). Localised canting models for substituted magnetic oxides. Journal of Physics C: Solid State Physics, 16(31), 5995.
72. Panicker, V. G., Upadhyay, R. V., Rao, S. N., & Kulkarni, R. G. (1984). Non-colinear spin structure in Ni-Cd ferrite system. J Mater Sci Lett 3, 385–387 (1984). https://doi.org/10.1007/BF00724373
73. H.J. Kardile, Sandeep B. Somvanshi, Apparao R. Chavan, A.A. Pandit, K.M. Jadhav, Effect of Cd2+ doping on structural, morphological, optical, magnetic and wettability properties of nickel ferrite thin films, Optik, Volume 207, 2020, 164462, ISSN 0030-4026, https://doi.org/10.1016/j.ijleo.2020.164462.
74. Safia Anjum, H.M. Tahir, K. Hussain, M. Khaleeq-ur-Rahman, M.S. Rafique, S. Naseem, Structural and magnetic properties of cadmium substituted Ni–Al ferrites, Physica B: Condensed Matter, Volume 406, Issue 13, 2011, Pages 2555-2558, ISSN 0921-4526, https://doi.org/10.1016/j.physb.2011.03.061.
75. Gongwen Gan, Dainan Zhang, Jie Li, Gang Wang, Xin Huang, Yan Yang, Yiheng Rao, Fang Xu, Xueying Wang, Huaiwu Zhang, Ray T. Chen, Equivalent permeability and permittivity of Sm substituted Mg–Cd ferrites for high-frequency applications, Journal of Alloys and Compounds, Volume 819, 2020, 153059, ISSN 0925-8388, https://doi.org/10.1016/j.jallcom.2019.153059.

76. S. S. Sikder, Saroaut Noor, M. A. Hakim, Per Nordblad, and Saiduzzaman , "Magnetization Behavior and Spin Canting in Diluted Co1−xCdxFe2O4 Ferrites", AIP Conference Proceedings 1347, 310-313 (2011) https://doi.org/10.1063/1.3601843
77. S. Akhter, M.A. Hakim, Magnetic properties of cadmium substituted lithium ferrites, Materials Chemistry and Physics, Volume 120, Issues 2–3, 2010, Pages 399-403, ISSN 0254-0584, https://doi.org/10.1016/j.matchemphys.2009.11.023.
78. Chetna C. Chauhan, Amrin R. Kagdi, Rajshree B. Jotania, Anupama Upadhyay, Charanjeet Singh Sandhu, Sagar E. Shirsath, Sher Singh Meena, Structural, magnetic and dielectric properties of Co-Zr substituted M-type calcium hexagonal ferrite nanoparticles in the presence of α-Fe2O3 phase, Ceramics International, Volume 44, Issue 15, 2018, Pages 17812-17823, ISSN 0272-8842, https://doi.org/10.1016/j.ceramint.2018.06.249.
79. Amrin R. Kagdi, Neha P. Solanki, Francisco E. Carvalho, Sher Singh Meena, Pramod Bhatt, Robert C. Pullar, Rajshree B. Jotania, Influence of Mg substitution on structural, magnetic and dielectric properties of X-type bariumzinc hexaferrites Ba2Zn2-xMgxFe28O46, Journal of Alloys and Compounds, Volume 741, 2018, Pages 377-391, ISSN 0925-8388, https://doi.org/10.1016/j.jallcom.2018.01.092.
80. Bammannavar, B.K. & Naik, L.R. & Pujar, R.B. & Chougule, B.K.. (2007). Preparation, characterization and physical properties of Mg-Zn ferrites. Indian Journal of Engineering and Materials Sciences. 14. 381-385.
81. F. Saffari, P. Kameli, M. Rahimi, H. Ahmadvand, H. Salamati, Effects of Co-substitution on the structural and magnetic properties of NiCoxFe2−xO4 ferrite nanoparticles, Ceramics International, Volume 41, Issue 6, 2015, Pages 7352-7358, ISSN 0272-8842, https://doi.org/10.1016/j.ceramint.2015.02.038.
82. T. Prabhakaran, J. Hemalatha, Chemical control on the size and properties of nano NiFe2O4 synthesized by sol–gel autocombustion method, Ceramics International, Volume 40, Issue 2, 2014, Pages 3315-3324, ISSN 0272-8842, https://doi.org/10.1016/j.ceramint.2013.09.103.
83. P. Geetha, Paulos Taddesse, N. Murali, P. V. Lakshmi Narayana, Impact of Gd3+ and Nd3+ ions substitution on structural and magnetic properties of Co0.5Ni0.5Fe2O4 ferrite system, Journal of the Indian Chemical Society, Volume 99, Issue 1, 2022, 100255, ISSN 0019-4522, https://doi.org/10.1016/j.jics.2021.100255.
84. K.S. Lohar, S.M. Patange, M.L. Mane, Sagar E. Shirsath, Cation distribution investigation and characterizations of $Ni_{1-x}Cd_xFe_2O_4$ nanoparticles synthesized by citrate gel process, Journal of Molecular Structure, Volume 1032, 2013, Pages 105-110, ISSN 0022-2860, https://doi.org/10.1016/j.molstruc.2012.07.055.
85. S. Oyarzún, A. Tamion, F. Tournus, V. Dupuis, M. Hillenkamp, Size efects in the magnetic anisotropy of embedded cobalt nanoparticles: from shape to surface. Sci. Rep. 5, 14749 (2015). https://doi.org/10.1038/srep14749
86. Rohit Sharma, Prashant Thakur, Manoj Kumar, Nagesh Thakur, N.S. Negi, Pankaj Sharma, Vineet Sharma, Improvement in magnetic behaviour of cobalt doped magnesium zinc nano-ferrites via co-precipitation route, Journal of Alloys and Compounds, Volume 684, 2016, Pages 569-581, ISSN 0925-8388, https://doi.org/10.1016/j.jallcom.2016.05.200.

87. Simi Debnath, Ratan Das, Cobalt doping on nickel ferrite nanocrystals enhances the micro-structural and magnetic properties: Shows a correlation between them, Journal of Alloys and Compounds, Volume 852, 2021, 156884, ISSN 0925-8388, https://doi.org/10.1016/j.jallcom.2020.156884.
88. Stefan Thamm, Jürgen Hesse, The remanence of a Stoner–Wohlfarth particle ensemble as a function of the demagnetisation process, Journal of Magnetism and Magnetic Materials, Volume 184, Issue 2, 1998, Pages 245-255, ISSN 0304-8853, https://doi.org/10.1016/S0304-8853(97)01135-9.
89. K. Maaz, S. Karim, A. Mashiatullah, J. Liu, M.D. Hou, Y.M. Sun, J.L. Duan, H.J. Yao, D. Mo, Y.F. Chen, Structural analysis of nickel doped cobalt ferrite nanoparticles prepared by coprecipitation route, Physica B: Condensed Matter, Volume 404, Issue 21, 2009, Pages 3947-3951, ISSN 0921-4526, https://doi.org/10.1016/j.physb.2009.07.134.
90. P.P. Hankare, K.R. Sanadi, R.S. Pandav, N.M. Patil, K.M. Garadkar, I.S. Mulla, Structural, electrical and magnetic properties of cadmium substituted copper ferrite by sol–gel method, Journal of Alloys and Compounds, Volume 540, 2012, Pages 290-296, ISSN 0925-8388, https://doi.org/10.1016/j.jallcom.2012.06.018.
91. Sathishkumar, G., Venkataraju, C. & Sivakumar, K. Magnetic and dielectric properties of cadmium substituted nickel cobalt nanoferrites. J Mater Sci: Mater Electron 24, 1057–1062 (2013). https://doi.org/10.1007/s10854-012-0878-3
92. Shyam Singh Thakur, Abhilash Pathania, Preeti Thakur, Atul Thakur, Jen-Hwa Hsu, Improved structural, electrical and magnetic properties of Mn-Zn-Cd nanoferrites, Ceramics International, Volume 41, Issue 3, Part B, 2015, Pages 5072-5078, ISSN 0272-8842, http://dx.doi.org/10.1016/j.ceramint.2014.12.077
93. Smit, J.; Wijn, H. P. J. Ferrites, John Wiley and Sons: New York, 1957, p. 157.
94. Adel Maher Wahba, Mohamed Bakr Mohamed, Structural, magnetic, and dielectric properties of nanocrystalline Cr-substituted Co0.8Ni0.2Fe2O4 ferrite, Ceramics International, Volume 40, Issue 4, 2014, Pages 6127-6135, ISSN 0272-8842, https://doi.org/10.1016/j.ceramint.2013.11.064.
95. G. Blasse, Ferromagnetism and ferrimagnetism of oxygen spinels containing tetravalent manganese, Journal of Physics and Chemistry of Solids, Volume 27, Issue 2, 1966, Pages 383-389, ISSN 0022-3697, https://doi.org/10.1016/0022-3697(66)90045-X.
96. V. Vasanthi, A. Shanmugavani, C. Sanjeeviraja, R. Kalai Selvan, Microwave assisted combustion synthesis of CdFe2O4: Magnetic and electrical properties, Journal of Magnetism and Magnetic Materials, Volume 324, Issue 13, 2012, Pages 2100-2107, ISSN 0304-8853, https://doi.org/10.1016/j.jmmm.2012.02.018.
97. P.N Vasambekar, C.B Kolekar, A.S Vaingankar, Magnetic behaviour of Cd2+ and Cr3+ substituted cobalt ferrites, Materials Chemistry and Physics, Volume 60, Issue 3, 1999, Pages 282-285, ISSN 0254-0584, https://doi.org/10.1016/S0254-0584(99)00062-0.